LIMNOLOGY
and
OCEANOGRAPHY

ASLO

Limnol. Oceanogr. 9999, 2020, 1–17

doi: 10.1002/lno.11419

Source partitioning of oxygen-consuming organic matter in the hypoxic zone of the Chesapeake Bay

Jianzhong Su,[1,2] Wei-Jun Cai ,[1*] Jean Brodeur ,[1] Najid Hussain ,[1] Baoshan Chen ,[1] Jeremy M. Testa ,[3] K. Michael Scaboo,[1] Deb P. Jaisi,[4] Qiang Li,[4] Minhan Dai ,[2] Jeffrey Cornwell [5]

[1]School of Marine Science and Policy, University of Delaware, Newark, Delaware
[2]State Key Laboratory of Marine Environmental Science, Xiamen University, Xiamen, China
[3]Chesapeake Biological Laboratory, University of Maryland Center for Environmental Science, Solomons, Maryland
[4]Department of Plant and Soil Sciences, University of Delaware, Newark, Delaware
[5]Horn Point Laboratory, University of Maryland Center for Environmental Science, Cambridge, Maryland

Abstract

We surveyed the carbonate system along the main channel of the Chesapeake Bay in June 2016 to elucidate carbonate dynamics and the associated sources of oxygen-consuming organic matter. Using a two endmember mixing calculation, chemical proxies, and stoichiometry, we demonstrated that in early summer, dissolved inorganic carbon (DIC) dynamics were controlled by aerobic respiration in the water column (43%), sulfate reduction in the sediment (39%), atmospheric CO_2 invasion (13%), and $CaCO_3$ dissolution (5%). A mass balance of the DIC concentration and its stable isotope suggested that the apparent $\delta^{13}C$ of oxygen-consuming organic matter was $-19.4 \pm 0.3‰$. The bulk composition of particulate organic matter also reflected a dominance of algal material (C/N = ~ 6, $\delta^{13}C > -25‰$). Therefore, we concluded that the decomposition of autochthonous organic matter (i.e., eutrophication-stimulated primary production) was the dominant process consuming oxygen, while allochthonous organic matter (terrestrially derived) made minor contributions to oxygen consumption in the hypoxic zone in June 2016. These findings in the Chesapeake Bay contrast with another hypoxic estuarine ecosystem, the Pearl River Estuary in China where allochthonous organic matter contributed significantly to oxygen consumption. The differences between these two systems in terms of hydrology, quantity and quality of organic matter, and physical characteristics are discussed to yield new insights on the formation and maintenance of hypoxia. In both systems, autochthonous organic matter dominates oxygen depletion, indicating that nutrient management and reduction are useful actions to control and mitigate the occurrence of hypoxia for the restoration of ecosystem.

Eutrophication-induced hypoxia in coastal waters has increased in spatial extent and severity in recent decades (Diaz and Rosenberg 2008; Breitburg et al. 2018). Respiration-driven reductions in bottom water oxygen are associated with CO_2 production and enhanced ocean acidification, threatening a variety of aquatic and benthic organisms and habitats (Wu 2002; Orr et al. 2005; Cai et al. 2011; Kroeker et al. 2013). Hypoxia is an outcome of an imbalance between oxygen supply and demand where water stratification physically inhibits oxygen replenishment from surface water allowing for organic matter (OM) remineralization to consume oxygen at a faster rate than reaeration of the bottom water (Rabouille et al. 2008; Testa et al. 2018*b*). Oxygen-consuming OM may originate from outside the aquatic system (i.e., allochthonous source) or be generated internally within the system (i.e., autochthonous source) (Paerl 2006; Rabalais et al. 2010). Allochthonous organic matter (Alloc-OC) typically originates from the watershed, including natural inputs such as vascular plant detritus, OM resulting from soil leaching and erosion, and anthropogenic inputs such as municipal and industrial wastewater, and agricultural runoff. In contrast, autochthonous organic matter (Autoc-OC) usually refers to eutrophication-stimulated primary production of phytoplankton within estuaries and the coastal oceans. Although many studies have demonstrated that highly reactive Autoc-OC dominates oxygen consumption in hypoxic waters (Turner and Rabalais 1994; Rabalais et al. 2014), others have suggested that the seemingly refractory, but occasionally abundant Alloc-OC may be more labile than previously thought due to a priming effect, and thus may also play an important role in oxygen depletion (Swarzenski et al. 2008; Bianchi 2011; Bianchi et al. 2011). The priming effect means the enhanced degradation of recalcitrant OM in the presence of possible

*Correspondence: wcai@udel.edu

priming substrates, such as phytoplankton exudates, heterotroph metabolites, and high nutrient cycle (Bianchi 2011), which eventually leads to the enhanced release of OM-derived carbon and nutrient as well as the enhanced consumption of oxygen. Quantifying the relative contributions of OM sources fueling oxygen consumption in the hypoxic zone allows for new insights on the formation and maintenance of hypoxia, while providing scientific support for regional management and policy-making for environmental restoration.

The Chesapeake Bay develops seasonal bottom water hypoxia and anoxia (Hagy et al. 2004; Murphy et al. 2011), due to a long water residence time of ~ 180 d (Du and Shen 2016), high retention of nutrients and OM, and high rates of internal Autoc-OC production (Fennel and Testa 2018). Previous studies have found that water column respiration dominates oxygen consumption, accounting for nearly two-thirds of the total respiration in below-pycnocline waters of the mid-Chesapeake Bay from April to August (Kemp et al. 1992; Li et al. 2016). The annual organic carbon budget for the Chesapeake Bay indicates that the input of Alloc-OC from rivers and the watershed is larger than Autoc-OC in the upper bay, while Autoc-OC represents most of the total organic carbon input in the mid-bay and lower bay (Biggs and Flemer 1972; Kemp et al. 1997; Shen et al. 2019*a*). The volume of hypoxic/anoxic water has a positive relationship with winter–spring river flow and nutrient loading (Hagy et al. 2004; Kemp et al. 2005), indicating Autoc-OC significantly contributes to respiration in the bay's hypoxic zone. However, observation-based studies have clearly shown either net heterotrophy or high CO_2 supersaturation in landward bay regions (Smith and Kemp 1995; Cai et al. 2017), and modeling studies have shown the organic loading from watershed and reservoir sediment scour during storm events can cause dissolved oxygen (DO) declines in the mainstem deep channel (Cerco and Noel 2016; Linker et al. 2016), both of which would suggest that Alloc-OC is important in some bay regions at some times. The extent to which this Alloc-OC influences the mid-bay region, especially if it is transported seaward in brief events, is unclear. Furthermore, the Chesapeake Bay is a local hotspot for sea level rise and associated shoreline erosion (Stevenson et al. 1985, 1988; Najjar et al. 2010). The extent to which OM originating from these eroding marshes is labile and reaches deeper mainstem waters also remains unknown. Therefore, a direct quantitative measurement of the relative contributions of Autoc-OC vs. Alloc-OC to oxygen consumption in the hypoxic zone of the Chesapeake Bay is needed to reinforce budget analyses and to improve our understanding of hypoxia drivers within the context of climate change (Najjar et al. 2010; Orth et al. 2017) and recent nutrient reductions (Lefcheck et al. 2018; Testa et al. 2018*b*).

In this study, we investigated the OM sources driving hypoxia formation and quantified the relative contribution of key respiration reactions involved in OM degradation using a suite of isotopic measures, chemical surveys, and mixing models. We adopted a two endmember mixing calculation to distinguish the biogeochemical processes from physical mixing in the Chesapeake Bay. Furthermore, chemical proxies and stoichiometry were used to quantify the rates of key biogeochemical processes, particularly sulfate reduction (SR), sulfide storage in the sediments, and atmospheric CO_2 invasion. Since aerobic respiration (AR) of OM produces dissolved inorganic carbon (DIC) with δ^{13}C-DIC similar to the isotope value of the respired OM (Hullar et al. 1996), we utilized a mass balance of DIC and its stable carbon isotope to trace the δ^{13}C of the respired substrate or oxygen-consuming OM in the hypoxic zone of the Chesapeake Bay. By combining those analyses with an examination of the bulk composition (C/N, δ^{13}C) of the particulate organic matter (POM) in the surface water of main channel as we previously did (Su et al. 2017), we were able to quantify the sources of oxygen-consuming OM. Finally, we compared the source partitioning results in the hypoxic zones of the Chesapeake Bay with the Pearl River Estuary (PRE), the largest estuary in southern China, in order to gain new insights on the formation and maintenance of hypoxia.

Materials and methods

Study site

The Chesapeake Bay (36.9°N–39.6°N, 75.5°W–77.5°W) is the largest estuary in the United States. The bay has a length of over 300 km, and a mean depth of 6.5 m (Kemp et al. 2005). The deep and narrow central channel is flanked by broad shallow areas, and the southern end is confined by a sill (Boicourt et al. 1999). The large watershed area and long dendritic bay shorelines make the bay susceptible to human disturbance, such as deforestation, agriculture, and urbanization. Eutrophication in the Chesapeake Bay began after European colonization in the 17th and 18th centuries (Brush 2009), and became more severe since the 1950s due to the growth in fertilizer use and other human activities in the watershed (Kemp et al. 2005). Nutrient loading increased steadily from the 1950s through the late-1980s (Hagy et al. 2004), after which loads stabilized and declined. Bay-wide water column nitrogen concentration has decreased by 23%, and phosphorus concentration has decreased by 8% from 1984 to 2015 (Lefcheck et al. 2018). Hypoxia typically begins in the late spring (late April and May) in the landward reaches of the bay's deep central basin, then expands seaward to occupy large regions of the main channel (Hagy et al. 2004; Testa and Kemp 2014). During the last three decades, the northward and winterward migration of the spring bloom has been associated with an increased volume of early season hypoxia, but a reduced late season volume and earlier hypoxia breakup (Murphy et al. 2011; Testa et al. 2018*b*).

Sampling and analytical methods

During 06–10 June 2016, we conducted a cruise aboard the R/V *Rachel Carson* along the bay's central axis that spanned the upper bay (CB2.1) southward to the bay mouth (AO1) (Fig. 1). During the cruise, we revisited the mid-bay Sta. 858 four times and Sta. CB4.3 twice.

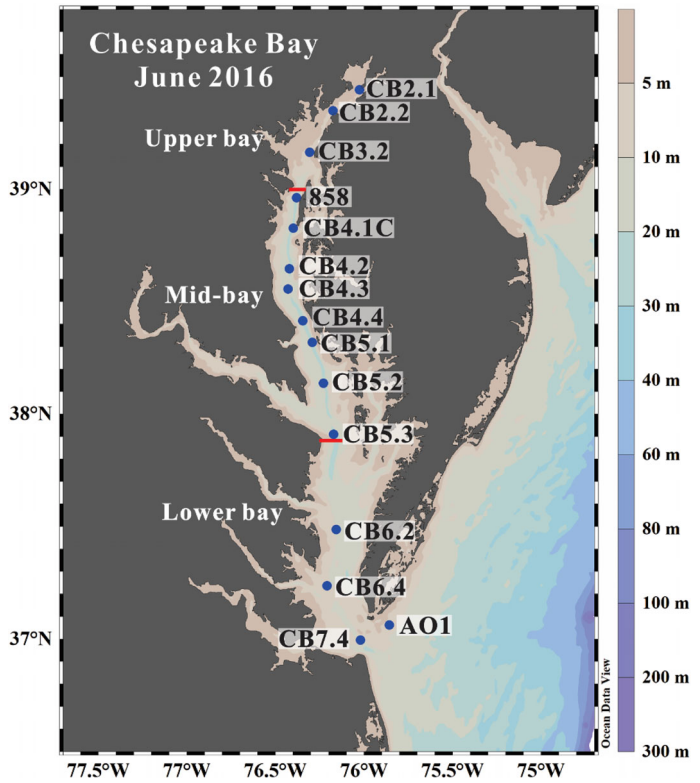

Fig. 1 Sampling locations along the main channel of the Chesapeake Bay in early June 2016. Following Kemp et al. (2005), we separated the main stem into three regions, that is, upper bay (39.0°N–39.5°N), mid-bay (37.9°N–39.0°N), and lower bay (37.0°N–37.9°N). The boundaries are noted with red lines.

At each station, we used a YSI 6600 attached to a submersible pump to obtain profiles of temperature, salinity, and O_2. Water was pumped from 2 to 7 depths to the deck for sampling, depending on the number of distinct water masses observed. We measured salinity separately in discrete total alkalinity TA and Ca^{2+} samples using a Cole-Parmer® salinity meter. For each depth, a water sample was preserved in a 250-mL borosilicate glass bottle with 50 μL saturated $HgCl_2$ solution for DIC and δ^{13}C-DIC analysis. For DIC, a 1 mL sample was acidified and the extracted CO_2 gas was subsequently quantified with an infrared CO_2 detector within 1 week after the cruise using a DIC analyzer (AS-C3, Apollo Scitech, U.S.A.) (Huang et al. 2012). The TA samples were not poisoned (Cai et al. 2017), and were analyzed within 24 h of collection using Gran titration in an open-cell setting (AS-ALK2, Apollo Scitech) (Cai et al. 2010*a*). The overall precision for DIC and TA was ± 0.1%. Both DIC and TA measurements were calibrated against Certified Reference Materials (CRMs) provided by Dr. A. G. Dickson at Scripps Institution of Oceanography (SIO), University of California, San Diego (UCSD). For δ^{13}C-DIC, a 3.8 mL sample was acidified in a gas stripper, CO_2 was extracted by a carrier gas, and the gas stream passed through a moisture condenser in a pretreatment device (AS-D1, Apollo Scitech) before measurement by a cavity ring-down spectrometer detector (G2131-i, Picarro, U.S.A.). A computer program was used to derive the δ^{13}C-DIC value by averaging the δ^{13}C-CO_2 at the stage when the simultaneously determined CO_2 concentration was high enough (> 100 ppm) for the detector to measure a stable δ^{13}C-CO_2 signal with little random noise. Two to three repeat runs were carried out for each sample, and a precision of 0.1‰ was achieved. A $NaHCO_3$ solution with known δ^{13}C-DIC value and CRMs were used for calibration. The details on analyzing δ^{13}C-DIC are described in Su et al. (2019).

We measured pH onboard using an Orion Ross glass electrode within 1 h after the water temperature was equilibrated to 25°C in a thermal water bath. Three NIST standards, that is, 4.01, 7.00, and 10.01, were used to calibrate the electrode. We analyzed discrete DO samples by direct spectrophotometry of total iodine following Pai et al. (1993) with a precision of ± 1 μmol kg^{-1}. Apparent oxygen utilization (AOU) was calculated by subtracting the measured DO from the saturated DO (Pilson 2012; Zhao et al. 2017). The DO solubility was calculated based on Benson and Krause (1984). We measured Ca^{2+} samples using a modified technique of Kanamori and Ikegami (1980) with a precision better than 0.1%. Note that the Ca^{2+} samples were measured in two batches. The upper and mid-bay samples were measured in the first batch, while the lower-bay samples (mostly salinity > 20) were measured in the second batch. Further analysis revealed that the deviation of Ca^{2+} (ΔCa^{2+}) relative to the conservative mixing line at salinity > 20 had greater noise than the data at salinity < 20, which may be due to reduced operating proficiency and electrode stability in the second batch. The pCO_2 was calculated from measured DIC and TA via a modified CO2SYS program with a H_2S component (Xu et al. 2017*a*). We derived the aragonite saturation state (Ω_{arag}) using measured Ca^{2+}, calculated CO_3^{2-}, and aragonite solubility based on Mucci (1983).

POM samples were collected in the surface water along the main channel in two cruises in June and August 2016. Samples were concentrated onto preweighed and precombusted 47 mm Whatman GF/F filters of 0.7 μm pore size after filtering 0.3–1.5 L water under a mild vacuum (~ 25 kPa). Filters were washed with distilled water and stored in a freezer. Before analysis, the filters were dried. Total suspended matter (TSM) was derived from the net weight increment on the filter and the filtration volume. Then, the filters were decarbonated with 1.0 mol L^{-1} HCl, and dried again at 40°C for 48 h (Kao et al. 2012). We analyzed the bulk composition (C, N, δ^{13}C) of POM samples on a DELTA V Plus isotope ratio mass spectrometer coupled with an elemental analyzer (Costech, CA). The stable isotope of particulate organic carbon (δ^{13}C-POC) was calibrated against two standard materials USGS40 (δ^{13}C = −26.39‰) and USGS41 (δ^{13}C = +37.63‰) with a precision of 0.1‰.

Two endmember mixing calculation

In estuarine research, a conservative mixing line of chemical concentrations against salinity between river and ocean endmembers is widely used to distinguish biogeochemical

alterations from physical water mixing (Officer 1979). Compared with the relatively consistent ocean endmember values, large variations exist in the river endmember mainly due to the temporal variations of freshwater discharge (Joesoef et al. 2017). For instance, mean monthly variations of DIC and TA in the Susquehanna River endmember of the Chesapeake Bay in 2016 were one-order of magnitude larger than the uncertainty of the estuarine endmember we adopted in this study (Table 1) (Brodeur et al. 2019). In addition, tributaries that discharge seaward of the Susquehanna River, such as the Chesapeake-Delaware Canal, may also introduce variability into DIC and TA concentrations. Since our focus is on the hypoxic zone in the mid-Chesapeake Bay, we decided to choose an estuarine endmember from the well-mixed upper bay instead of the traditional river endmember. We considered CB2.2 to be a representative endmember, because it is a well-mixed station in a narrow section of the upper bay before the bay widens downstream, and there are no adjacent major tributaries. Further considering the large slope value of measured Ca^{2+} against salinity (Fig. 3b), a small salinity difference between the surface layer (salinity = 3.0) and bottom layer (salinity = 3.9) at Sta. CB2.2 would result in a significant difference on Ca^{2+}. Therefore, we adopted the measured values in the low salinity layer (surface) rather than the averaged values of the whole water column at CB2.2 as the estuarine endmember in the upper bay. For the offshore seawater endmember, we first developed linear regressions of DIC, TA, and Ca^{2+} against salinity (DIC = 79 × Salinity − 596, R^2 = 0.72, $p < 0.0001$; TA = 54 × Salinity + 428, R^2 = 0.99, $p < 0.0001$; Ca^{2+} = 269 × Salinity + 831, R^2 = 0.98, $p < 0.0001$) with data from four stations (82, 83, 85, and 87) in the Mid-Atlantic Bight, which were visited during the East Coast Ocean Acidification (ECOA) cruise in July 2015 (Xu et al. 2017*b*). Then, we used the salinity of the ocean endmember (33.618 ± 0.139) from Cai et al. (2017) to derive the offshore endmember values for our June 2016 cruise. According to the latitude range of the Chesapeake Bay (36°N–40°N), we adopted the offshore δ^{13}C-DIC endmember value as 1.3 ± 0.1‰ based on Quay et al. (2007), who compiled multiyear δ^{13}C-DIC data to delineate meridional trends of δ^{13}C-DIC in the surface Atlantic Ocean during the 1980s to 2000s. Both the offshore seawater DIC and δ^{13}C-DIC endmember values fall within the ranges in the Mid-Atlantic Bight reported by Bauer et al. (2001). All the endmember values and uncertainties are summarized in Table 1.

Then, considering the mid-bay and lower bay water as a mixture between estuarine water in CB2.2 and offshore seawater, we calculated the mixing fractions of the two endmembers based on the following equations:

$$f_{\mathrm{estu}} = \frac{S_{\mathrm{sw}} - S_{\mathrm{meas}}}{S_{\mathrm{sw}} - S_{\mathrm{estu}}} \quad (1)$$

$$f_{\mathrm{sw}} = 1 - f_{\mathrm{estu}} \quad (2)$$

where S is salinity; f represents the mixing fraction; the subscripts estu and sw indicate the estuarine and seawater endmember, respectively, and meas denotes the measured value. These fractions were then used to predict conservative concentrations (i.e., $[X]_{\mathrm{con}}$) of certain chemical constituents (i.e., DIC, TA, or Ca^{2+}) resulting solely from two endmember mixing:

$$[X]_{\mathrm{con}} = [X]_{\mathrm{estu}} \times f_{\mathrm{estu}} + [X]_{\mathrm{sw}} \times f_{\mathrm{sw}} \quad (3)$$

The difference between measured and conservative values is defined as total nonconservative value of $[X]$ (i.e., $\Delta[X]_{\mathrm{total}}$) (Fig. 3c):

$$\Delta[X]_{\mathrm{total}} = [X]_{\mathrm{meas}} - [X]_{\mathrm{con}} \quad (4)$$

The positive or negative $\Delta[X]_{\mathrm{total}}$ indicates addition or removal of $[X]$ to the water column, which is a composite result driven by multiple biogeochemical processes, such as AR and $CaCO_3$ dissolution (CD). Similarly, the conservative δ^{13}C-DIC value in the bay resulting from physical mixing of the upper estuarine water and the seawater is:

$$\delta^{13}\mathrm{C}_{\mathrm{DICcon}} = \frac{\delta^{13}\mathrm{C}_{\mathrm{DICestu}} \times \mathrm{DIC}_{\mathrm{estu}} \times f_{\mathrm{estu}} + \delta^{13}\mathrm{C}_{\mathrm{DICsw}} \times \mathrm{DIC}_{\mathrm{sw}} \times f_{\mathrm{sw}}}{\mathrm{DIC}_{\mathrm{con}}} \quad (5)$$

Results and discussion

Distribution of chemical constituents along the main channel

Spatial patterns of physical and chemical conditions in June 2016 reveal substantial variations along the salinity gradient. The surface-water temperature was generally higher than the bottom water temperature (Fig. 2a), where in the

Table 1. Summary of endmember values and their uncertainties.

Endmembers	Salinity	DIC (μmol kg^{-1})	δ^{13}C-DIC (‰)	TA (μmol kg^{-1})	Ca^{2+} (mmol kg^{-1})
CB2.2	2.8 ± 0.1	965 ± 2	−6.8 ± 0.1	929 ± 2	1.246 ± 0.010*
Offshore	33.6 ± 0.1	2063 ± 11	1.3 ± 0.1†	2245 ± 8	9.884 ± 0.037

*Additional salinity measurements were performed on the Ca^{2+} samples (salinity = 3.0 ± 0.1).
†Cited from Quay et al. (2007).

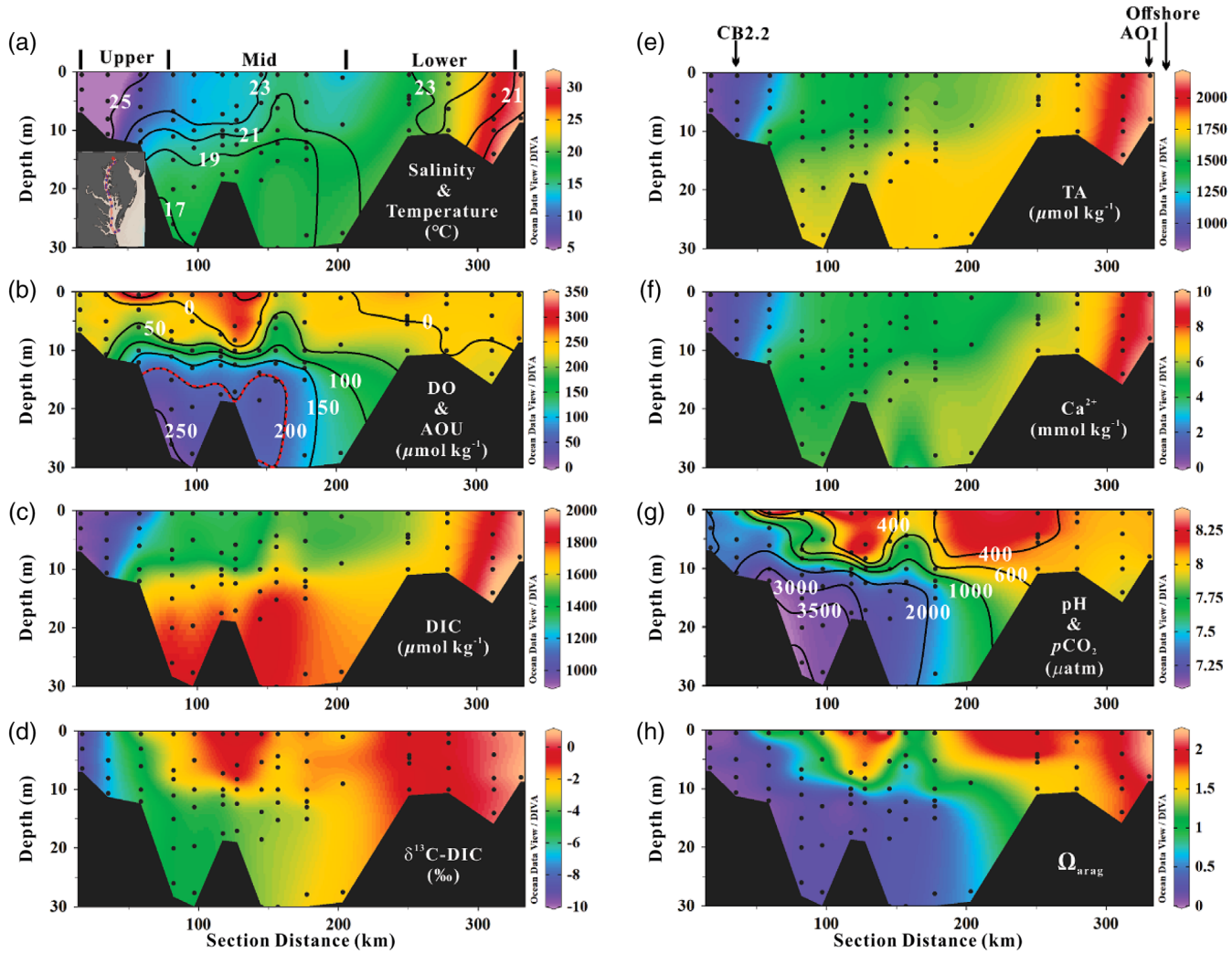

Fig. 2 Sectional distributions of water properties in the main channel of the Chesapeake Bay in early June 2016. (**a**) Salinity (color) and contours of temperature, (**b**) DO (color) and contours for AOU, (**c**) DIC, (**d**) δ^{13}C-DIC, (**e**) TA, (**f**) Ca^{2+}, (**g**) pH (NBS, 25°C) and contours for pCO_2, and (**h**) Ω_{arag}. Note that the red dash curve shows the boundary of hypoxic zone, where DO is less than 63 μmol kg^{-1}. The geological location of this section extending from Sta. CB2.1 in the northern bay southward to the bay mouth (Fig. 1). Offshore stations were not included in the section profiles, because they are located much more offshore in the Mid-Atlantic Bight.

mid-bay, the average temperature in the surface water (23.2 ± 1.1°C) was ~ 5°C higher than in the bottom water (17.9 ± 0.9°C). A two-layer estuarine circulation can clearly be seen from the salinity distribution (Fig. 2a), that is, fresher water flows seaward in the surface, while saline water intrudes landward in the bottom. The salinity gradient contributed to the majority (> 90%) of the density stratification (Goodrich et al. 1987; Kemp et al. 1992), with a pycnocline depth at ~ 10 m inferred from sectional distributions of salinity and DO in Fig. 2a,b. Below the pycnocline, there was a hypoxic zone in the mid-bay with the lowest DO of 21 μmol kg^{-1} observed at Sta. 858. A DO supersaturation zone was observed in the surface water immediately above the hypoxic zone, with the highest DO of 327 μmol kg^{-1} (equivalent to 133% of saturated DO or −81 μmol kg^{-1} of AOU) observed at Sta. CB3.2, indicating a close spatial coupling between sub-pycnocline AR and surface primary production (Fig. 2b). Carbonate dynamics were also coupled to oxygen in the hypoxic zone and phytoplankton bloom zone. In the bottom hypoxic zone, DIC and pCO_2 were enriched (Fig. 2c, g), while δ^{13}C-DIC, pH, and Ω_{arag} were lower (Fig. 2d,g,h). In the surface phytoplankton bloom zone, however, the opposite pattern was observed: DIC and pCO_2 decreased, and δ^{13}C-DIC, pH, and Ω_{arag} increased. The distributions of TA and Ca^{2+} generally followed the pattern of salinity (Fig. 2e,f). The pH and Ω_{arag} remained low in the upper bay and in mid-bay bottom water, but were higher in more saline, seaward waters (Fig. 2g,h). H_2S was also measured at each station and depth, but concentrations were all below the detection limit (0.5 μmol L^{-1}).

Apparent sources of DIC and TA in the hypoxic zone

DIC and TA behaved in a nearly conservative way in both the upper and lower bay, but large quantities of DIC and TA were added to the mid-bay water column, with peak addition values of 344 μmol kg^{-1} and 161 μmol kg^{-1}, respectively (Fig. 3c). AOU was low in the upper bay (< 50 μmol kg^{-1}), increased significantly up to 250 μmol kg^{-1} in the below-pycnocline water of the mid-bay, and was near equilibrium (~ 0 μmol kg^{-1}) with the atmosphere in the lower bay water (Fig. 2b). Nonconservative Ca^{2+} (ΔCa^{2+}) was close to zero at salinity < 10, but increased up to 50 μmol kg^{-1} at salinity 10~20 (Fig. 3c), suggesting moderate CD occurred in the mid-bay water. Beyond salinity 20, ΔCa^{2+} had greater noise than that at salinity < 20 probably because of reduced operating proficiency and electrode stability during sample analysis. Since the general pattern of Ca^{2+} against salinity was correct (Fig. 3b), and the maximum non-conservative deviation value (ΔCa^{2+} = −61 μmol kg^{-1}) was small compared with the corresponding measured Ca^{2+} values (4245–9373 μmol kg^{-1}), we retained the Ca^{2+} and ΔCa^{2+} data at salinity > 20 in Fig. 3b,c as open circles, but excluded those data in further calculations.

Assuming the oxidation state of organic carbon is zero, the AR of OM characterized with a Redfield ratio (C : N : P = 106:16:1) would result in a stoichiometry of ΔDIC_{AR} : ΔTA_{AR} : AOU = 106: −17:138 (Table 2). Note that H_3PO_4 is a strong acid, and donates a proton in its contribution to TA (Wolf-Gladrow et al. 2007; Cai et al. 2010*b*). Carbonate dissolution releases Ca^{2+} and increases DIC and TA with a stoichiometry of ΔDIC_{CD} : ΔTA_{CD} : ΔCa^{2+} = 1:2:1 (Table 2). Given that we can directly estimate AOU and ΔCa^{2+}, as well as their related chemical stoichiometry, first we can calculate the DIC and TA changes caused by AR (ΔDIC_{AR} = 106 × [AOU/138] and ΔTA_{AR} = −17 × [AOU/138]) and CD (ΔDIC_{CD} = ΔCa^{2+} and ΔTA_{CD} = 2 × ΔCa^{2+}). Then, we subtracted the DIC and TA changes of these two processes from the total nonconservative values (ΔDIC_{total} and ΔTA_{total}). The residual DIC and TA (i.e., $\Delta DIC_{total\text{-}CD\text{-}AR}$ and $\Delta TA_{total\text{-}CD\text{-}AR}$) are significantly different from zero (Fig. 4), indicating that AR and CD cannot fully explain the additions of DIC and TA in the mid-bay water column. Previous studies on coastal hypoxia have shown that in addition to the dominance of AR, other processes can significantly influence the carbonate dynamics, such as nitrification in the upper reach of the PRE (Dai et al. 2008; He et al. 2014)

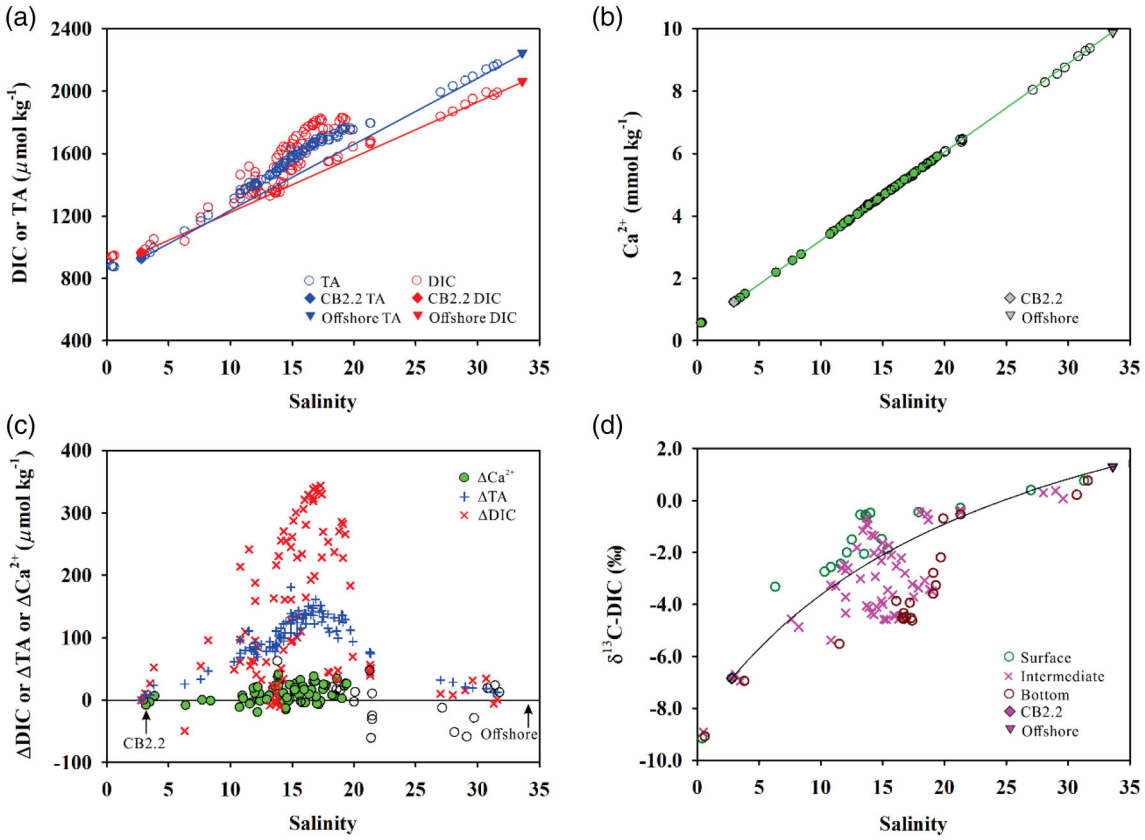

Fig. 3 Total alkalinity, DIC and its stable isotope, calcium ion against salinity, and their deviations from the conservative mixing lines. We calculated mixing lines between CB2.2 (the estuarine endmember) and offshore seawater (the oceanic endmember) to assess the nonconservative behaviors of (**a**) TA, DIC, (**b**) Ca^{2+}, and (**d**) δ^{13}C-DIC. The deviation values of TA, DIC, and Ca^{2+} are presented in (**c**). Note that there is a zero reference line and the endmembers are marked by arrows. The open circles in (**b**) and (**c**) represent the lower-bay Ca^{2+} and ΔCa^{2+} data, which were measured in the second batch.

Table 2. Biogeochemical processes that affect the stoichiometric ratios of DIC and TA.

Processes	Reaction equations	ΔTA/ΔDIC
AR	$(CH_2O)_{106}(NH_3)_{16}(H_3PO_4) + 138O_2 \rightarrow 106CO_2 + 16HNO_3 + H_3PO_4 + 122H_2O$	−(16 + 1)/106 = −0.16
CD	$CaCO_3 + CO_2 + H_2O \rightarrow Ca^{2+} + 2HCO_3^-$	2/1
SR*	$(CH_2O)_{106}(NH_3)_{16}(H_3PO_4) + 53SO_4^{2-} \rightarrow 106HCO_3^- + 53H_2S + 16NH_3 + H_3PO_4$	(106 + 16-1)/106 = 1.14
Sulfide oxidation	$H_2S + 2O_2 \rightarrow SO_4^{2-} + 2H^+$	−2/0
Sulfide storage†	$Fe(OH)_3 + 1/2H_2S + 2H^+ \rightarrow Fe^{2+} + 1/2S + 3H_2O$	2/0
	$Fe^{2+} + H_2S \rightarrow FeS + 2H^+$	−2/0
	$FeS + H_2S \rightarrow FeS_2 + H_2$	0/0

*Cited from Cai et al. (2017).
†Cited from Rassmann et al. (2019).

and oxidation of reduced chemical species in the water column in the Black Sea and Cariaco basin (Millero 1991*a*; Rabalais et al. 2010). Considering that the mid-bay is typically where gross primary production, respiration (plankton + benthic), and SR peak

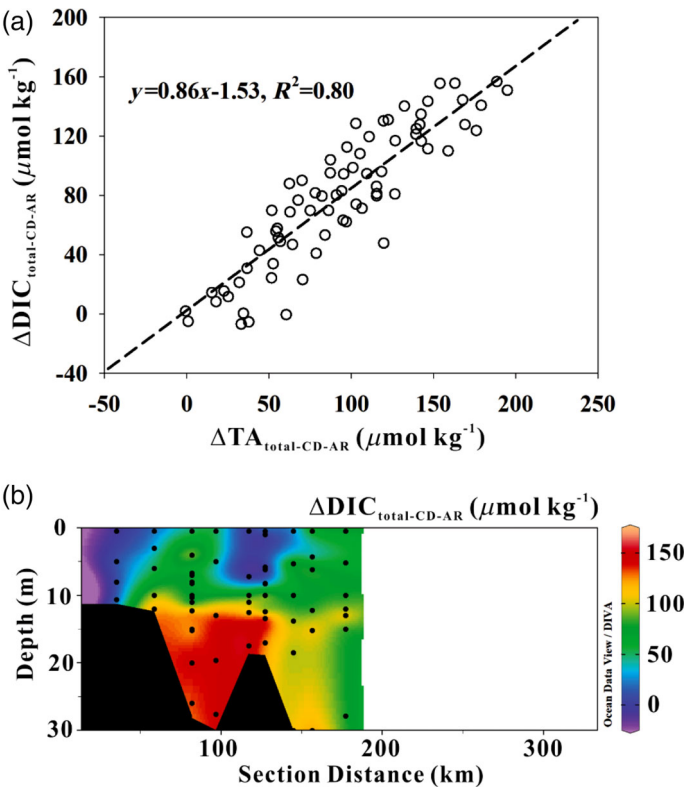

Fig. 4 (**a**) The ratio of nonconservative DIC and TA excluding the portion related to CD and AR, and (**b**) the sectional distribution of the nonconservative DIC values.

(Kemp et al. 1997), while surface pCO_2 is undersaturated with respect to the atmosphere in spring and summer (Cai et al. 2017), it is clear that SR and atmospheric CO_2 invasion could be alternative contributors to carbonate system dynamics. These two contributors will be discussed in the next two sections.

SR and sulfide storage in the sediment

We inferred that SR in the mid-bay sediment had a significant influence on the carbonate system in the water column based on three lines of evidence. First, the residual DIC and TA (i.e., $\Delta DIC_{total\text{-}CD\text{-}AR}$ and $\Delta TA_{total\text{-}CD\text{-}AR}$) are generally positive and have a ratio of 0.86 with a high R^2 of 0.80 in the mid-bay (Fig. 4a), which approximates the ratio of DIC and TA changes induced by SR (0.88) (Table 2). Second, the vertical distribution of $\Delta DIC_{total\text{-}CD\text{-}AR}$ does show higher values in deep water than in surface water, suggesting this residual DIC originates from the sediment (Fig. 4b). However, no H_2S was detected in June 2016, while low but detectable O_2 was observed in bottom water, indicating no significant SR in the water column. Previous studies have demonstrated that SR (60–80%) and AR (20–40%) appear to be the most important pathways for organic carbon mineralization in mid-bay sediments at ≥ 10 m water depth (Burdige and Homstead 1994; Roden et al. 1995). Alternative metabolic pathways (nitrification and methanogenesis) occur at relatively low rates in the mid-bay in summer (Kemp et al. 1990; Hill et al. 1992; Brady et al. 2013; Testa et al. 2013), while much of the metal oxide reduction is dominated by interaction with sulfide, rather than oxidation of sedimentary OM (Burdige 1993; Lustwerk and Burdige 1993).

In the mid-bay sediments during summer, sulfide production rates via SR typically exceed sulfide oxidation rates (Roden and Tuttle 1992; Roden et al. 1995), suggesting sulfide storage in the sediments (Sampou and Oviatt 1991) or release to the overlying bottom water (Roden and Tuttle 1993). During our cruise in June 2016, we did not observe H_2S accumulation in the water column of the hypoxic zone, indicating that H_2S released from the sediment was rapidly oxidized (Millero 1991*b*). Oxidation of H_2S by O_2 would not change DIC, but it could consume a considerable fraction of the TA produced by SR (Table 2). If all of the SR-generated H_2S diffused upward and was oxidized by O_2, we would have found the sediments to be a source for DIC, and a weak sink for TA. In contrast, our data show substantial additions of both DIC and TA from the sediment to the water column (Fig. 4), indicating that a major proportion of H_2S was removed (or stored) in the sediment below the oxic layer. Previous observations in mid-bay sediments have revealed a dynamic seasonal cycle of iron sulfide accumulation during summer and reoxidation in winter (Cornwell and Sampou 1995). Since the abiotic reduction of iron oxides by H_2S coupled with either FeS or pyrite precipitation does not overall alter TA (Table 2) (Rassmann et al. 2019), this will not influence the ratio of DIC and TA produced by

bacterial SR, which leads to the slope value nearly identical to 0.88 (Fig. 4a).

Based on published data for SR rates, sediment-water fluxes, and several related assumptions, we estimated the changes to DIC and TA concentrations resulting from sediment SR for comparison with our calculated $\Delta DIC_{total\text{-}CD\text{-}AR}$ (0–160 μmol kg^{-1}) and $\Delta TA_{total\text{-}CD\text{-}AR}$ (0–200 μmol kg^{-1}) (Fig. 4a). To make these calculations, we assumed (1) a mid-bay SR rate in June between 15.6 and 70.3 mmol S m^{-2} d^{-1} (Kemp et al. 1997), (2) the ratio of sulfide storage to total SR was 20% on an annual basis (Roden and Tuttle 1993), (3) an average height of 20 m for the whole water column, and (4) a water residence time of 120 d for the mid-bay water (Du and Shen 2016). Provided these assumptions, we estimated that SR followed by sulfide storage would result in a DIC addition of 38–169 μmol L^{-1} and a TA addition of 43–193 μmol L^{-1} to the water column, comparable to what were derived from our observation-based estimates. Furthermore, previous studies have reported that the measured sediment-water fluxes of DIC were 16~84 mmol m^{-2} d^{-1} in the mid-bay in summer (Burdige and Homstead 1994; Burdige and Zheng 1998; Lee et al. 2015). In June, the benthic DIC flux of 30~42 mmol m^{-2} d^{-1} is equivalent to 180~252 μmol L^{-1} DIC addition to the water column under the same assumptions as above, suggesting that SR followed by sulfide storage could largely explain the residual DIC and TA addition ($\Delta DIC_{total\text{-}CD\text{-}AR}$ and $\Delta TA_{total\text{-}CD\text{-}AR}$) that we derived using stoichiometric balances.

AR and atmospheric CO_2 invasion

In addition to AR, oxidation of reduced chemicals (e.g., H_2S, Mn^{2+}, Fe^{2+}) mixing upward from the sediment–water interface also consumes oxygen in the water column. Therefore, it is not strictly correct to use AOU and the theoretical ratio of $\Delta DIC_{AR}/AOU$ (i.e., 106/138 = 0.77) to derive the DIC addition via AR of OM. Assuming the stoichiometric ratios of $\Delta TA/\Delta DIC$ for SR (= 1.14) and AR (= –0.16) are valid (Table 2), we developed a mass balance of DIC and TA to independently derive their changes induced by AR, and further examined its actual $\Delta DIC_{AR}/AOU$ ratio. We used x and y to represent the quantities of DIC addition via SR and AR, respectively, and thus the TA changes would be 1.14x for SR and –0.16y for AR.

$$\Delta DIC_{total} - \Delta DIC_{CD} = x + y \quad (6)$$

$$\Delta TA_{total} - \Delta TA_{CD} = 1.14x - 0.16y \quad (7)$$

Then, the quantity of SR-induced DIC addition was resolved as x and noted as $\Delta DIC_{SR(x1)}$. The actual DIC addition induced by AR was resolved as y and noted as $\Delta DIC_{total\text{-}CD\text{-}SR(x1)}$. As shown in Fig. 5, the $\Delta DIC_{total\text{-}CD\text{-}SR(x1)}/AOU$ ratio is 0.61 (Fig. 5), and is close to the Redfield ratio of 0.77 (Redfield 1934), indicating AR of OM dominated the DO consumption in the water column.

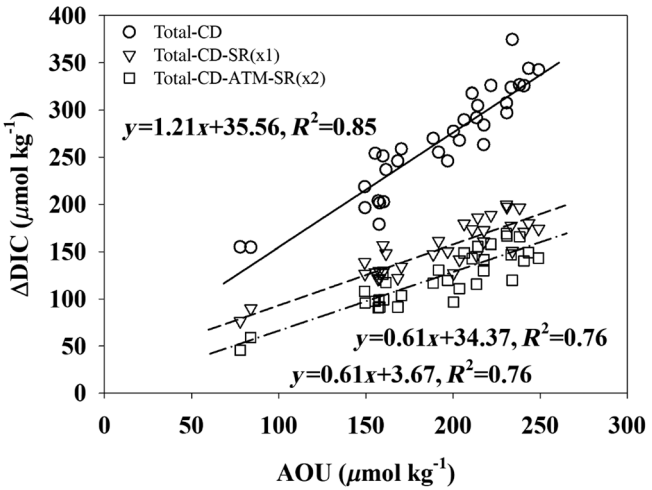

Fig. 5 The different types of nonconservative DIC plotted against AOU in the below-pycnocline water in the mid-bay. The total-CD refers to the total ΔDIC minus the portion caused by CD. The total-CD-SR(x1) means the part of nonconservative DIC induced by the process excluding CD and SR, which is noted as SR(x1) without considering atmospheric CO_2 invasion. Similarly, the total-CD-ATM-SR(x2) indicates the part of nonconservative DIC generated by the process excluding CD, SR, and atmospheric CO_2 invasion. More details about SR(x1) and SR(x2) are in the "Discussion" section.

The positive intercepts of $\Delta DIC_{total\text{-}CD}$ and $\Delta DIC_{total\text{-}CD\text{-}SR(x1)}$ against AOU for the below-pycnocline water in the mid-bay, however, mean that there was another DIC source unrelated to oxygen consumption (Fig. 5). As shown in Fig. 2g, the pCO_2 in the mid-bay surface water was below the atmospheric level (~ 400 μatm), and should have caused atmospheric CO_2 invasion, which may have contributed to water column CO_2 accumulation (Cai et al. 2017). The intercept value of ~ 35 μmol kg^{-1} is very close to the bottom-water DIC changes induced by atmospheric CO_2 invasion estimated by Cai et al. (2017) (~ 21–33 μmol kg^{-1}) and modeled by Shen et al. (2019*b*) (~ 20.4–52.3 μmol kg^{-1}). Thus, we suggest that the invasion of atmospheric CO_2 is another important control on water-column DIC, and its alteration on DIC is noted as ΔDIC_{ATM}. Assuming ΔDIC_{ATM} equals 35 μmol kg^{-1} throughout the water column, and CO_2 invasion does not influence TA, we can recalculate the DIC addition via AR and SR by using the modified Eq. 6 (i.e., $\Delta DIC_{total} - \Delta DIC_{CD} - \Delta DIC_{ATM} = x + y$) and the same Eq. 7 (i.e., $\Delta TA_{total} - \Delta TA_{CD} = 1.14x - 0.16y$). For this time, the SR-induced DIC addition was noted as $\Delta DIC_{SR(x2)}$, while the AR-induced DIC addition was noted as $\Delta DIC_{total\text{-}CD\text{-}ATM\text{-}SR(x2)}$. Here, the regression of $\Delta DIC_{total\text{-}CD\text{-}ATM\text{-}SR(x2)}$ against AOU has a similar slope but a much smaller intercept value, which is not statistically different from zero (n = 33, p > 0.05) (Fig. 5). In order to illustrate the following calculations neatly, the subscripts of $\Delta DIC_{SR(x2)}$, and $\Delta DIC_{total\text{-}CD\text{-}ATM\text{-}SR(x2)}$ were simplified as SR and AR in Eqs. 8–12.

The apparent $\delta^{13}C$ value of oxygen-consuming OM

We have shown that in early June, the nonconservative DICs in the below-pycnocline water of the mid-bay are controlled by AR,

CD, sedimentary SR, and the invasion of atmospheric CO_2 (ATM). This allows us to construct a mass balance equation for DIC:

$$\Delta DIC_{total} = \Delta DIC_{CD} + \Delta DIC_{ATM} + \Delta DIC_{SR} + \Delta DIC_{AR} \quad (8)$$

By dividing the DIC changes from each process by ΔDIC_{total}, we further quantified that CD, ATM, SR, and AR accounted for 5%, 13%, 39%, and 43%, respectively, of the total non-conservative DIC in the below-pycnocline waters of the mid-bay. However, the distribution of δ^{13}C-DIC was more than a result of DIC concentration change, but also influenced by the distinct δ^{13}C source values and isotopic fractionation of individual biogeochemical process (Alling et al. 2012; Samanta et al. 2015; Su et al. 2019). In contrast to the DIC addition in the mid-bay subsurface water, the correlated δ^{13}C-DIC values were beneath the isotopic mixing line (Fig. 3d), indicating a considerable proportion of DIC addition was ^{13}C-depleted. Therefore, similar to DIC, we derived a mass balance equation for the stable carbon isotope of DIC:

$$\begin{aligned} &\delta^{13}C_{DICmeas} \times DIC_{meas} - \delta^{13}C_{DICcon} \times DIC_{con} \\ &= \delta^{13}C_{DIC_{CD}} \times \Delta DIC_{CD} + \delta^{13}C_{DIC_{ATM}} \times \Delta DIC_{ATM} \\ &+ \delta^{13}C_{DIC_{SR}} \times \Delta DIC_{SR} + \delta^{13}C_{DIC_{AR}} \times \Delta DIC_{AR} \end{aligned} \quad (9)$$

To derive the isotope value of oxygen-consuming OM from Eq. 9 as well as Eqs. 1, 3, 5, and 8, a few assumptions or approximations are needed. The sources of $CaCO_3$ that dissolved in the water column may include marine limestone, abiotic precipitation, and biogenic calcification. In another study described in a manuscript currently under review, we show that $CaCO_3$ formation driven by submerged aquatic vegetation and shell organisms may play an important role in supplying $CaCO_3$ for further dissolution in the subsurface water of the mid-bay to lower bay (J. Su unpubl.). However, the sources and δ^{13}C values of these $CaCO_3$ solids have not yet been quantified in the Chesapeake Bay. Considering CD only accounted for 5% of the DIC addition in early June 2016, the uncertainty introduced by δ^{13}C-DIC_{CD} must be rather small. Thus, we tentatively assume the δ^{13}C-DIC_{CD} to be 0‰, which is widely used to represent marine limestone (Craig 1953; Presley and Kaplan 1968).

Yet, the invasion of atmospheric CO_2 would also cause isotopic fractionation between the atmospheric CO_2 and added DIC. Given the average temperature (20.6 $\pm$ 2.4°C) in the mid-bay water column, the fractionation factor could be calculated as −9.4‰ following Samanta et al. (2015). Assuming the δ^{13}C of atmospheric CO_2 was −8‰, we can derive the δ^{13}C of CO_2-invasion-induced DIC (δ^{13}C-DIC_{ATM}) as 1.4‰. AR and SR both degrade OM, but use different terminal electron acceptors, that is, O_2 vs. SO_4^{2-}. Aerobic degradation of OM typically produces DIC with minor isotopic fractionation from the substrate OM (Hullar et al. 1996; Breteler et al. 2002; Lehmann et al. 2002). Previous studies indicate that degradation of marine POM via SR is a nonfractionating process, and have adopted the δ^{13}C of POM undergoing degradation as the δ^{13}C value of the end-product DIC (Irwin et al. 1977; Komada et al. 2016; Fernandes et al. 2018). Therefore, the isotopic composition of DIC_{AR} (i.e., $\delta^{13}C_{AR}$) and DIC_{SR} (i.e., $\delta^{13}C_{SR}$) should be identical to the δ^{13}C of substrate OM (i.e., $\delta^{13}C_{OCx}$), which consumes oxygen or sulfate and produces DIC to the water column. Thus, the $\delta^{13}C_{OCx}$ could be derived from the following equation:

$$\delta^{13}C_{OCx} = \frac{\delta^{13}C_{DICmeas} \times DIC_{meas} - \delta^{13}C_{DICcon} \times DIC_{con} - \delta^{13}C_{DIC_{CD}} \times \Delta DIC_{CD} - \delta^{13}C_{DIC_{ATM}} \times \Delta DIC_{ATM}}{DIC_{meas} - DIC_{con} - \Delta DIC_{CD} - \Delta DIC_{ATM}} \quad (10)$$

where DIC_{con} and $\delta^{13}C_{DICcon}$ could be calculated from Eqs. 3, 4, ΔDIC_{CD} equals to the deviation of Ca^{2+} (i.e., ΔCa^{2+}), and ΔDIC_{ATM} equals 35 μmol kg^{-}1 throughout the water column. The propagated errors of the calculated $\delta^{13}C_{OCx}$ can be estimated following Wang et al. (2018). The composite uncertainty of the derived $\delta^{13}C_{OCx}$ was $\pm$3.8‰, which was the potential maximum uncertainty when propagating all errors from the endmembers and measurements. Combining Eqs. 9, 10, we can get the following equation:

$$\delta^{13}C_{AR} \times \Delta DIC_{AR} + \delta^{13}C_{SR} \times \Delta DIC_{SR} = \delta^{13}C_{OCx} \times (\Delta DIC_{AR} + \Delta DIC_{SR}) \quad (11)$$

Note that ΔDIC_{AR} (= $\Delta DIC_{total\text{-}CD\text{-}ATM\text{-}SR(x2)}$) and ΔDIC_{SR} (= $\Delta DIC_{SR(x2)}$) are known, and $\delta^{13}C_{OCx}$ (= $\delta^{13}C_{AR}$ = $\delta^{13}C_{SR}$) can be calculated for each sample by Eq. 10. Unlike the codominance of AR and SR as well as a moderate contribution from CD and ATM to DIC and $\delta^{13}C_{DIC}$ dynamics in the Chesapeake Bay, AR is the most important biogeochemical process controlling DIC and $\delta^{13}C_{DIC}$ in the PRE (Su et al. 2017). In order to compare the magnitude of AR-induced DIC change and the apparent origin of oxygen-consuming OM in the two systems, we extracted the portion only induced by AR from Eq. 11 and expressed that as:

$$\Delta(\delta^{13}C_{DIC} \times DIC) = \delta^{13}C_{OCx} \times \Delta DIC_{AR} \quad (12)$$

The term at the left side of Eq. 12 means the product of $\delta^{13}C_{OCx}$ (= $\delta^{13}C_{AR}$) and ΔDIC_{AR} for each sample. When we

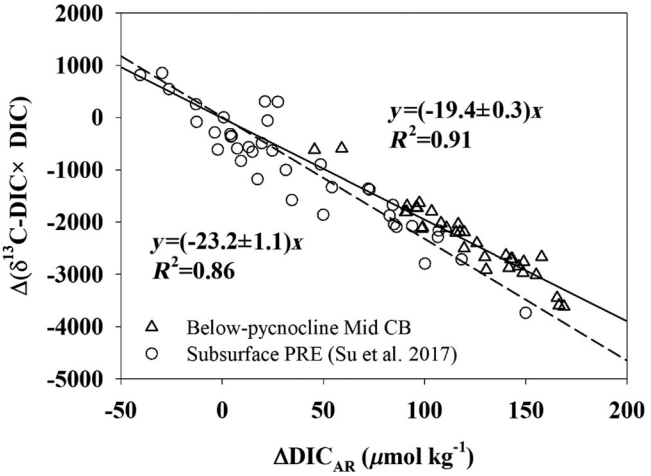

Fig. 6 The $\Delta(\delta^{13}C\text{-}DIC \times DIC)$ vs. ΔDIC_{AR} in the below-pycnocline water of the mid-Chesapeake Bay. The slope reflects the original $\delta^{13}C$ signature of oxygen-consuming OM undergoing remineralization ($\delta^{13}C_{OCx}$). The PRE data set is from Su et al. (2017).

plot $\Delta(\delta^{13}C_{DIC} \times DIC)$ against ΔDIC_{AR} (Fig. 6), the slope value of $-19.4 \pm 0.3‰$ reflects the apparent $\delta^{13}C$ signature of oxygen-consuming OM undergoing remineralization. Note that the uncertainty of the slope (± 0.3‰) is directly derived from the linear regression in Fig. 6, which is much smaller than the potential maximum composite uncertainty of the derived $\delta^{13}C_{OCx}$ (± 3.8‰). In this case, we used marine limestone as the $CaCO_3$ source ($\delta^{13}C\text{-}DIC_{CD} = 0‰$). However, Grimm et al. (2017) once measured the $\delta^{13}C$ of oyster shells in the James River estuary, one of the tributaries in the southwestern Chesapeake Bay, which ranged from −7.6‰ to 0.5‰ and had a positive relationship with salinity. Even if $\delta^{13}C\text{-}DIC_{CD}$ varies from −8‰ to 1‰ as measured for oyster shells (Grimm et al. 2017), the slope value changes little from −19.0‰ to −19.5‰, which is within the uncertainty of the slope using $\delta^{13}C\text{-}DIC_{CD} = 0‰$. Therefore, in our case, the slope value is not sensitive to the variation of $\delta^{13}C\text{-}DIC_{CD}$ because carbonate dissolution contributed only a small fraction (~ 5%) to the DIC addition in early June 2016. Assuming the isotopic composition of OM is conservative or regulated only by physical mixing, this apparent $\delta^{13}C_{OCx}$ could be seen as a mixing signal from two distinct endmember sources, that is, Autoc-OC and Alloc-OC (Thornton and McManus 1994).

Source partitioning of oxygen-consuming OM

We verified the relative contributions of Autoc-OC and Alloc-OC by examining the bulk composition of POM and defining the isotopic endmember values (Shultz and Calder 1976; Thornton and McManus 1994; Yu et al. 2010). TSM showed a decreasing trend from the upper (~ 13 mg kg^{-1}) to the lower bay (~ 4 mg kg^{-1}) (Fig. 7a), while POC sharply increased in the southern portion of the upper bay, and then decreased seaward (Fig. 7b). The peak POC value occurred at

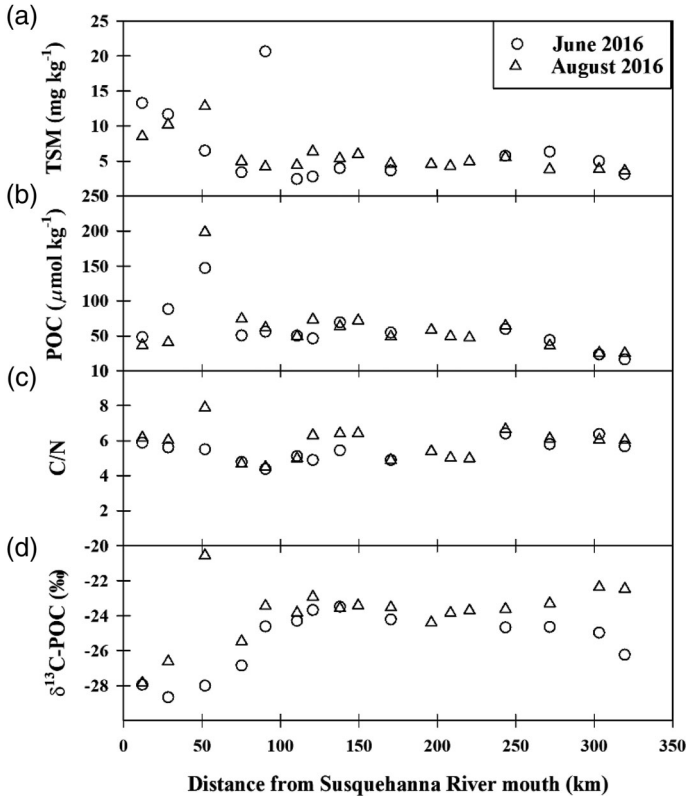

Fig. 7 Spatial distribution of (**a**) TSM, (**b**) POC, (**c**) molar C/N ratio, and (**d**) $\delta^{13}C$-POC along the main channel of the Chesapeake Bay in June (circle) and August (triangle) 2016. TSM and POC concentrations are expressed in per kilogram water units.

CB3.2, which had the highest DO (327 μmol kg^{-1}) and chlorophyll *a* concentration (16.0 $\mu g\ L^{-1}$), indicating that the POC increase was caused by strong primary production and associated phytoplankton biomass. The molar C/N ratio varied from 4.4 to 7.9, with an average value close to 6 (Fig. 7c), similar to the results of Byonton and Kemp (1985) (4.0–13.0), Horrigan et al. (1990) (6.9–12.2), Canuel and Zimmerman (1999) (4.8–9.1), Sigleo and Macko (2002) (7.0–12.0), and Loh et al. (2006) (~ 6.0). The $\delta^{13}C$-POC values generally increased southward and had a range of −28.7‰ to −20.6‰ (Fig. 7d), similar to the results of Canuel (2001) (−27.8‰ to −19.9‰), Sigleo and Macko (2002) (−26.9‰ to −17.5 ‰), and Loh et al. (2006) (−28.0‰ to −21.4‰).

In this study, the distributions of C/N and $\delta^{13}C$ demonstrate that Autoc-OC (estuarine/marine phytoplankton) constitutes a major portion of POM in the mid-bay to lower bay. This is supported by our findings of C/N ratios close to 6 and $\delta^{13}C > -25‰$ along the majority of meso- and polyhaline waters where hypoxia exists. Our findings of low Alloc-OC (terrestrial) influence is not surprising given that the winter–spring (January–May) river flow in 2016 was 20% lower than the long-term average (1967–2017) and freshwater input was at a seasonal minimum during our cruise period (Fig. 8b).

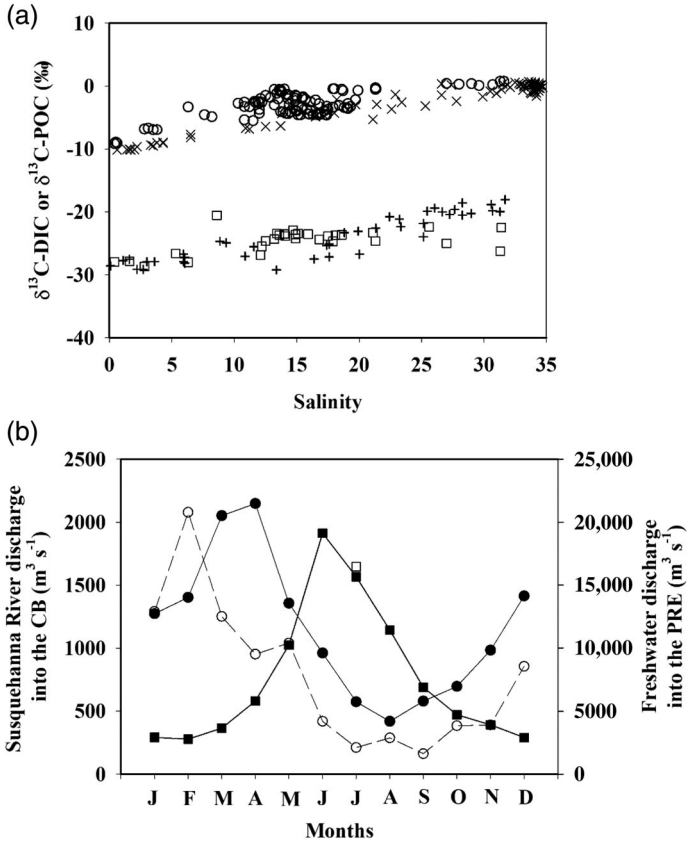

Fig. 8 Comparisons of δ^{13}C-DIC, δ^{13}C-POC, and freshwater discharge between the Chesapeake Bay and the PRE. In panel (**a**), the open circles and squares represent the δ^{13}C-DIC (June) and δ^{13}C-POC (June + August) from the CB cruises in 2016. For the PRE, the crosses are the δ^{13}C-DIC values from July 2014, whereas the pluses are the δ^{13}C-POC values from July 2015. The PRE data are from Su et al. (2017). In panel (**b**), the filled circles indicate the monthly average freshwater discharge rate for the Susquehanna River at Conowingo Dam (USGS site number 01578310) during 1967–2017, while the open circles refer to 2016. The Susquehanna River supplies 50–60% of mean annual freshwater input to the Chesapeake Bay (Schubel and Pritchard 1986; Testa et al. 2018*a*). The filled and open squares show the monthly average freshwater discharges in the PRE during multiple years (2000–2011) and July 2014, respectively.

These low flow conditions likely allowed any imported, terrestrial OM and freshwater phytoplankton to be trapped in the upper-bay turbidity maximum zone (Sanford et al. 2001; Cheng et al. 2013).

When we combined the lowest δ^{13}C-POC values in our study with three previous studies (Canuel 2001; Sigleo and Macko 2002; Loh et al. 2006), we derived a δ^{13}C-POC value of -27.9 ± 0.7‰ as the endmember for Alloc-OC (terrestrial) or freshwater algae. Similarly, using the highest δ^{13}C-POC values in these four studies, we derived a δ^{13}C-POC endmember value for Autoc-OC (marine) of -19.9 ± 1.7‰. Therefore, our derived δ^{13}C of oxygen-consuming OM (-19.4 ± 0.3‰) is within the uncertainty of the Autoc-OC isotopic signal. The fact that oxygen-consuming OM signal is the approximate value of marine OM may reflect rapid settling and/or landward intrusion of marine-derived OM from the high salinity regions, consistent with well-known estuarine circulation patterns (Arzayus and Canuel 2005). Previous studies have demonstrated that the water of the continental shelf, flowing into the bay's mouth, is the largest single source of sediment for the Chesapeake Bay (Meade 1969; Hobbs III et al. 1992). Moreover, the $\delta^{13}C_{OCx}$ may be influenced by the high organic content (as high as 74% [dry weight] in the marsh sediment) and more ^{13}C-enriched (~ −12.5‰) materials eroded from the marshes (Stevenson et al. 1985; Stribling and Cornwell 1997). Nonetheless, we did not find any POM sample with such a ^{13}C-enriched signal in our cruises (Figs. 7d, 8a). In addition, the absence of biomarkers associated with terrestrial and marsh sources in summer precludes the possibility that admixture of terrestrial and marsh materials accounts for a major portion of OM that consumes oxygen (Canuel 2001; Loh et al. 2006). However, we cannot exclude the possible contributions of terrestrial and marsh materials to oxygen-consuming OM pool in other periods, especially during high-flow seasons (winter and spring) and storm events (Stevenson et al. 1988; Canuel 2001). Overall, our results demonstrate that eutrophication-stimulated primary production (Autoc-OC) dominated oxygen-consuming OM pool in the hypoxic zone of the Chesapeake Bay in June 2016.

Comparison with hypoxia in the lower reach of the PRE

It is useful to compare our isotopic analysis in the Chesapeake Bay (CB) with similar recent measurements in the PRE (21.2°N–23.1°N, 113.0°E–114.5°E), a large subtropical estuarine system in southern China. The PRE also receives large amounts of nutrient and OM loadings (Zhang et al. 1999; Cai et al. 2004; Dai et al. 2006), and suffers from severe eutrophication (Huang et al. 2003). Recent observations suggest that the lower PRE has emerged as a seasonal hypoxic zone (Qian et al. 2018). Unlike the CB, with persistent summer hypoxia occurring at > 10 m depth (Hagy et al. 2004), the lower PRE hypoxic zone is highly variable given a short water residence time of only a few days and strong tidal and wind mixing, especially during typhoon events (Su et al. 2017). Despite these differences, oxygen consumption in both systems is dominated by AR of Autoc-OC (~ 100% in the CB vs. ~ 65% in the PRE), while Alloc-OC is also a significant contributor (~ 35%) to oxygen consumption in the PRE (Su et al. 2017). The δ^{13}C-POC values were similar in both estuaries near the freshwater zone, but differed in the seawater regions (Fig. 8a), likely due to additional tributary OM inputs to the lower CB (Arzayus and Canuel 2005; Countway et al. 2007). Finally, the δ^{13}C-DIC values measured during summer were generally higher or more positive in the CB than in the PRE (Fig. 8a), presumably because variations in carbonate weathering in the watershed and different biogeochemistry within the bay waters, such as CD and atmospheric CO_2 invasion. In the mid-CB, there is atmospheric CO_2 uptake because of the strong drawdown of surface pCO_2 driven by photosynthesis and long water residence time. In contrast, within the PRE, supersaturated

Table 3. Comparison of the Chesapeake Bay and the Pearl River Estuary in terms of hydrology, quantity and quality of organic matter input, and physical characteristics.

	Chesapeake Bay	Pearl River Estuary
Annual freshwater discharge ($\times 10^9$ m^3 yr^{-1})	73*	350[†]
Timing of peak freshwater discharge	Mar or Apr	Jun
Estuarine water volume ($\times 10^9$ m^3)	75[‡]	8[§]
Water residence time (d)	180[‡]	3–5[‖]
Annual sediment loads ($\times 10^6$ tons yr^{-1})	4.3[¶]	85[†]
Primary productivity (g C m^{-2} d^{-1})	1–9[#]	1–5[‖]
Bioavailability of Alloc-OC	—**	Relatively high[††]
Water temperature in hypoxic zone (°C)	17.0–18.5[‡‡]	23.7–27.6[§§]

*Kemp et al. (2005).
[†]Zhang et al. (1999).
[‡]Du and Shen (2016).
[§]Guan et al. (2009).
[‖]Rabouille et al. (2008).
[¶]Langland and Cronin (2003).
[#]Officer et al. (1984).
**This study shows that there is little contribution from Alloc-OC to oxygen consumption in the hypoxic zone of the Chesapeake Bay.
[††]Strong et al. (2012).
[‡‡]This study.
[§§]Su et al. (2017).

pCO_2 in the surface water and short water residence time lead to no CO_2 uptake into the water (Guo et al. 2009).

To interpret why terrestrial OM contributes significantly to the oxygen consumption in the PRE but not in the CB, we have to consider the differences in terms of hydrology, quantity and quality of both Alloc-OC and Autoc-OC, and the physical setting. As shown in Table 3, the CB has a smaller annual freshwater input, about one-fifth of that in the PRE, but has an estuarine water volume ~ 10 times as large as that in the PRE. That leads to a much longer water residence time in the CB. Considering the smaller annual sediment loads in the CB, most of the Alloc-OC likely settles in the upper bay (Biggs 1970; Boynton and Kemp 1985; Cheng et al. 2013), except in the high discharge period of March or April (Fig. 8b). Thus, in summer, when freshwater discharge is low (Fig. 8b), little terrestrial OM reaches the mid-bay and lower bay, and Autoc-OC composes most of the OM pool in the CB. In contrast, the much larger annual sediment loads and much shorter water residence time in the PRE enables considerable terrestrial OM be transported to the shallow shelf region, where bottom hypoxia develops. This terrestrial OM delivery would be more substantial during the peak freshwater discharge in the PRE in summer when our measurements were made (Fig. 8b). There appears to be substantial amounts of bioavailable OM in both systems, but the OM is substantially influenced by Alloc-OC that is exposed to minor degradative loss during the short transport period in the PRE (Strong et al. 2012), while Autoc-OC is far more important in the CB, which is generally more productive (1–9 g C m^{-2} d^{-1}) than the PRE (1–5 g C m^{-2} d^{-1}) (Officer et al. 1984; Rabouille et al. 2008). Finally, the temperature of the hypoxic water in the PRE (23.7–27.6°C) was higher than that in the CB (17.0–18.5°C), which favors higher rates of bacterial growth and OM degradation (Brown et al. 2004), allowing for potentially higher rates of terrestrial OM degradation within the hypoxic zone of the lower PRE. Clearly, the two large hypoxic zones in these estuarine systems have substantially different physical features and sources of OM input and lability, suggesting that future analyses are required to better understand the varied drivers of hypoxia across coastal systems worldwide.

References

Alling, V., D. Porcelli, C. M. Mörth, L. G. Anderson, L. Sanchez-Garcia, Ö. Gustafsson, P. S. Andersson, and C. Humborg. 2012. Degradation of terrestrial organic carbon, primary production and out-gassing of CO_2 in the Laptev and East Siberian Seas as inferred from $\delta^{13}C$ values of DIC. Geochim. Cosmochim. Acta **95**: 143–159. doi:10.1016/j.gca.2012.07.028

Arzayus, K. M., and E. A. Canuel. 2005. Organic matter degradation in sediments of the York River estuary: Effects of biological vs. physical mixing. Geochim. Cosmochim. Acta **69**: 455–464. doi:10.1016/j.gca.2004.06.029

Bauer, J. E., E. R. M. Druffel, D. M. Wolgast, and S. Griffin. 2001. Sources and cycling of dissolved and particulate organic radiocarbon in the Northwest Atlantic Continental Margin. Global Biogeochem. Cycles **15**: 615–636. doi:10.1029/2000GB001314

Benson, B. B., and D. Krause. 1984. The concentration and isotopic fractionation of oxygen dissolved in freshwater and seawater in equilibrium with the atmosphere. Limnol. Oceanogr. **29**: 620–632. doi:10.4319/lo.1984.29.3.0620

Bianchi, T. S. 2011. The role of terrestrially derived organic carbon in the coastal ocean: A changing paradigm and the priming effect. Proc. Natl. Acad. Sci. USA **108**: 19473–19481. doi:10.1073/pnas.1017982108

Bianchi, T. S., L. A. Wysocki, K. M. Schreiner, T. R. Filley, D. R. Corbett, and A. S. Kolker. 2011. Sources of terrestrial organic carbon in the Mississippi plume region: Evidence for the importance of coastal marsh inputs. Aquat. Geochem. **17**: 431–456. doi:10.1007/s10498-010-9110-3

Biggs, R. B. 1970. Sources and distribution of suspended sediment in northern Chesapeake Bay. Mar. Geol. **9**: 187–201. doi:10.1016/0025-3227(70)90014-9

Biggs, R. B., and D. A. Flemer. 1972. The flux of particulate carbon in an estuary. Mar. Biol. **12**: 11–17. doi:10.1007/bf00347425

Boicourt, W. C., M. Kuzmić, and T. S. Hopkins. 1999. The inland sea: Circulation of Chesapeake Bay and the Northern Adriatic, p. 81–129. *In* T. C. Malone, A. Malej, L. W. Harding Jr., N. Smodlaka, and R. E. Turner [eds.], Ecosystems at the land-sea margin: Drainage basin to coastal sea. American Geophysical Union.

Boynton, W., and W. M. Kemp. 1985. Nutrient regeneration and oxygen consumption by sediments along an estuarine salinity gradient. Mar. Ecol. Prog. Ser. **23**: 45–55. doi:10.3354/meps023045

Brady, D. C., J. M. Testa, D. M. Di Toro, W. R. Boynton, and W. M. Kemp. 2013. Sediment flux modeling: Calibration and application for coastal systems. Estuar. Coast. Shelf Sci. **117**: 107–124. doi:10.1016/j.ecss.2012.11.003

Breitburg, D., and others. 2018. Declining oxygen in the global ocean and coastal waters. Science **359**: eaam7240. doi:10.1126/science.aam7240

Breteler, W. C. K., K. Grice, S. Schouten, H. T. Kloosterhuis, and J. S. S. Damsté. 2002. Stable carbon isotope fractionation in the marine copepod *Temora longicornis*: Unexpectedly low $\delta^{13}C$ value of faecal pellets. Mar. Ecol. Prog. Ser. **240**: 195–204. doi:10.3354/meps240195

Brodeur, J. R., and others. 2019. Chesapeake Bay inorganic carbon: Spatial distribution and seasonal variability. Front. Mar. Sci. **6**: 99. doi:10.3389/fmars.2019.00099

Brown, J. H., J. F. Gillooly, A. P. Allen, V. M. Savage, and G. B. West. 2004. Toward a metabolic theory of ecology. Ecology **85**: 1771–1789. doi:10.1890/03-9000

Brush, G. S. 2009. Historical land use, nitrogen, and coastal eutrophication: A paleoecological perspective. Estuaries Coast. **32**: 18–28. doi:10.1007/s12237-008-9106-z

Burdige, D. J. 1993. The biogeochemistry of manganese and iron reduction in marine sediments. Earth Sci. Rev. **35**: 249–284. doi:10.1016/0012-8252(93)90040-E

Burdige, D. J., and J. Homstead. 1994. Fluxes of dissolved organic carbon from Chesapeake Bay sediments. Geochim. Cosmochim. Acta **58**: 3407–3424. doi:10.1016/0016-7037(94)90095-7

Burdige, D. J., and S. Zheng. 1998. The biogeochemical cycling of dissolved organic nitrogen in estuarine sediments. Limnol. Oceanogr. **43**: 1796–1813. doi:10.4319/lo.1998.43.8.1796

Cai, W.-J., and others. 2004. The biogeochemistry of inorganic carbon and nutrients in the Pearl River estuary and the adjacent Northern South China Sea. Cont. Shelf Res. **24**: 1301–1319. doi:10.1016/j.csr.2004.04.005

Cai, W.-J., X. Hu, W.-J. Huang, L.-Q. Jiang, Y. Wang, T.-H. Peng, and X. Zhang. 2010*a*. Alkalinity distribution in the western North Atlantic Ocean margins. J. Geophys. Res. Oceans **115**: C08014. doi:10.1029/2009JC005482

Cai, W.-J., G. W. Luther, J. C. Cornwell, and A. E. Giblin. 2010*b*. Carbon cycling and the coupling between proton and electron transfer reactions in aquatic sediments in Lake Champlain. Aquat. Geochem. **16**: 421–446. doi:10.1007/s10498-010-9097-9

Cai, W.-J., and others. 2011. Acidification of subsurface coastal waters enhanced by eutrophication. Nat. Geosci. **4**: 766–770. doi:10.1038/NGEO1297

Cai, W.-J., and others. 2017. Redox reactions and weak buffering capacity lead to acidification in the Chesapeake Bay. Nat. Commun. **8**: 369. doi:10.1038/s41467-017-00417-7

Canuel, E. A. 2001. Relations between river flow, primary production and fatty acid composition of particulate organic matter in San Francisco and Chesapeake Bays: A multivariate approach. Org. Geochem. **32**: 563–583. doi:10.1016/S0146-6380(00)00195-9

Canuel, E. A., and A. R. Zimmerman. 1999. Composition of particulate organic matter in the southern Chesapeake Bay: Sources and reactivity. Estuaries **22**: 980–994. doi:10.2307/1353077

Cerco, C. F., and M. R. Noel. 2016. Impact of reservoir sediment scour on water quality in a downstream estuary. J. Environ. Qual. **45**: 894–905. doi:10.2134/jeq2014.10.0425

Cheng, P., M. Li, and Y. Li. 2013. Generation of an estuarine sediment plume by a tropical storm. J. Geophys. Res. Oceans **118**: 856–868. doi:10.1002/jgrc.20070

Cornwell, J. C., and P. A. Sampou. 1995. Environmental controls on iron sulfide mineral formation in a coastal plain estuary, p. 224–242. *In* M. A. Vairavamurthy, M. A. A. Schoonen, T. I. Eglinton, G. W. Luther III, and B. Manowitz [eds.], Geochemical transformations of sedimentary sulfur. American Chemical Society.

Countway, R. E., E. A. Canuel, and R. M. Dickhut. 2007. Sources of particulate organic matter in surface waters of the York River, VA estuary. Org. Geochem. **38**: 365–379. doi:10.1016/j.orggeochem.2006.06.004

Craig, H. 1953. The geochemistry of the stable carbon isotopes. Geochim. Cosmochim. Acta **3**: 53–92. doi:10.1016/0016-7037(53)90001-5

Dai, M., and others. 2006. Oxygen depletion in the upper reach of the Pearl River estuary during a winter drought. Mar. Chem. **102**: 159–169. doi:10.1016/j.marchem.2005.09.020

Dai, M., L. Wang, X. Guo, W. Zhai, Q. Li, B. He, and S.-J. Kao. 2008. Nitrification and inorganic nitrogen distribution in a large perturbed river/estuarine system: The Pearl River Estuary, China. Biogeosciences **5**: 1227–1244. doi:10.5194/bg-5-1227-2008

Diaz, R. J., and R. Rosenberg. 2008. Spreading dead zones and consequences for marine ecosystems. Science **321**: 926–929. doi:10.1126/science.1156401

Du, J., and J. Shen. 2016. Water residence time in Chesapeake Bay for 1980–2012. J. Mar. Syst. **164**: 101–111. doi:10.1016/j.jmarsys.2016.08.011

Fennel, K., and J. M. Testa. 2018. Biogeochemical controls on coastal hypoxia. Ann. Rev. Mar. Sci. **11**: 4.1–4.26. doi:10.1146/annurev-marine-010318-095138

Fernandes, S., and others. 2018. Enhanced carbon-sulfur cycling in the sediments of Arabian Sea oxygen minimum zone center. Sci. Rep. **8**: 8665. doi:10.1038/s41598-018-27002-2

Goodrich, D. M., W. C. Boicourt, P. Hamilton, and D. W. Pritchard. 1987. Wind-induced destratification in Chesapeake Bay. J. Phys. Oceanogr. **17**: 2232–2240. doi:10.1175/1520-0485(1987)017<2232:widicb>2.0.co;2

Grimm, B., H. Spero, J. Harding, and T. Guilderson. 2017. Seasonal radiocarbon reservoir ages for the 17th century James River, Virginia estuary. Quat. Geochronol. **41**: 119–133. doi:10.1016/j.quageo.2017.03.002

Guo, X., M. Dai, W. Zhai, W.-J. Cai, and B. Chen. 2009. CO_2 flux and seasonal variability in a large subtropical estuarine system, the Pearl River Estuary, China. J. Geophys. Res. **114**: G03013. doi:10.1029/2008JG000905

Hagy, J. D., W. R. Boynton, C. W. Keefe, and K. V. Wood. 2004. Hypoxia in Chesapeake Bay, 1950–2001: Long-term change in relation to nutrient loading and river flow. Estuaries **27**: 634–658. doi:10.1007/BF02907650

He, B., M. Dai, W. Zhai, X. Guo, and L. Wang. 2014. Hypoxia in the upper reaches of the Pearl River Estuary and its maintenance mechanisms: A synthesis based on multiple year observations during 2000–2008. Mar. Chem. **167**: 13–24. doi:10.1016/j.marchem.2014.07.003

Hill, J. M., J. P. Halka, R. Conkwright, K. Koczot, and S. Coleman. 1992. Distribution and effects of shallow gas on bulk estuarine sediment properties. Cont. Shelf Res. **12**: 1219–1229. doi:10.1016/0278-4343(92)90081-T

Hobbs, C. H., III, J. P. Halka, R. T. Kerhin, and M. J. Carron. 1992. Chesapeake Bay sediment budget. J. Coast. Res. **8**: 292–300.

Horrigan, S. G., J. P. Montoya, J. L. Nevins, J. J. McCarthy, H. Ducklow, R. Goericke, and T. Malone. 1990. Nitrogenous nutrient transformations in the spring and fall in the Chesapeake Bay. Estuar. Coast. Shelf Sci. **30**: 369–391. doi:10.1016/0272-7714(90)90004-B

Huang, W. J., Y. Wang, and W. J. Cai. 2012. Assessment of sample storage techniques for total alkalinity and dissolved inorganic carbon in seawater. Limnol. Oceanogr.: Methods **10**: 711–717. doi:10.4319/lom.2012.10.711

Huang, X., L. Huang, and W. Yue. 2003. The characteristics of nutrients and eutrophication in the Pearl River estuary, South China. Mar. Pollut. Bull. **47**: 30–36. doi:10.1016/S0025-326X(02)00474-5

Hullar, M., B. Fry, B. Peterson, and R. Wright. 1996. Microbial utilization of estuarine dissolved organic carbon: A stable isotope tracer approach tested by mass balance. Appl. Environ. Microbiol. **62**: 2489–2493.

Irwin, H., C. Curtis, and M. Coleman. 1977. Isotopic evidence for source of diagenetic carbonates formed during burial of organic-rich sediments. Nature **269**: 209–213. doi:10.1038/269209a0

Joesoef, A., D. L. Kirchman, C. K. Sommerfield, and W.-J. Cai. 2017. Seasonal variability of the inorganic carbon system in a large coastal plain estuary. Biogeosciences **14**: 4949–4963. doi:10.5194/bg-14-4949-2017

Kanamori, S., and H. Ikegami. 1980. Computer-processed potentiometric titration for the determination of calcium and magnesium in sea water. J. Oceanogr. Soc. Jpn. **36**: 177–184. doi:10.1007/bf02070330

Kao, S.-J., Terence Yang, J.-Y., Liu, K.-K., Dai, M., Chou, W.-C., Lin, H.-L., and Ren, H. 2012. Isotope constraints on particulate nitrogen source and dynamics in the upper water column of the oligotrophic South China Sea. Global Biogeochem. Cycles **26**: GB2033. doi:10.1029/2011GB004091

Kemp, W. M., P. Sampou, J. Caffrey, M. Mayer, K. Henriksen, and W. R. Boynton. 1990. Ammonium recycling versus denitrification in Chesapeake Bay sediments. Limnol. Oceanogr. **35**: 1545–1563. doi:10.4319/lo.1990.35.7.1545

Kemp, W. M., P. A. Sampou, J. Garber, J. Tuttle, and W. R. Boynton. 1992. Seasonal depletion of oxygen from bottom waters of Chesapeake Bay: Roles of benthic and planktonic respiration and physical exchange processes. Mar. Ecol. Prog. Ser. **85**: 137–152. doi:10.3354/meps085137

Kemp, W. M., E. M. Smith, M. Marvin-DiPasquale, and W. R. Boynton. 1997. Organic carbon balance and net ecosystem metabolism in Chesapeake Bay. Mar. Ecol. Prog. Ser. **150**: 229–248. doi:10.3354/meps150229

Kemp, W. M., and others. 2005. Eutrophication of Chesapeake Bay: Historical trends and ecological interactions. Mar. Ecol. Prog. Ser. **303**: 1–29. doi:10.3354/meps303001

Komada, T., D. J. Burdige, H.-L. Li, C. Magen, J. P. Chanton, and A. K. Cada. 2016. Organic matter cycling across the sulfate-methane transition zone of the Santa Barbara Basin, California Borderland. Geochim. Cosmochim. Acta **176**: 259–278. doi:10.1016/j.gca.2015.12.022

Kroeker, K. J., R. L. Kordas, R. Crim, I. E. Hendriks, L. Ramajo, G. S. Singh, C. M. Duarte, and J. P. Gattuso. 2013. Impacts of ocean acidification on marine organisms: Quantifying sensitivities and interaction with warming. Glob. Chang. Biol. **19**: 1884–1896. doi:10.1111/gcb.12179

Lee, D. Y., M. S. Owens, M. Doherty, E. M. Eggleston, I. Hewson, B. C. Crump, and J. C. Cornwell. 2015. The effects of oxygen transition on community respiration and potential chemoautotrophic production in a seasonally stratified anoxic estuary. Estuaries Coast. **38**: 104–117. doi:10.1007/s12237-014-9803-8

Lefcheck, J. S., and others. 2018. Long-term nutrient reductions lead to the unprecedented recovery of a temperate coastal region. Proc. Natl. Acad. Sci. USA **115**: 3658–3662. doi:10.1073/pnas.1715798115

Lehmann, M. F., S. M. Bernasconi, A. Barbieri, and J. A. McKenzie. 2002. Preservation of organic matter and alteration of its carbon and nitrogen isotope composition during simulated and in situ early sedimentary diagenesis.

Geochim. Cosmochim. Acta **66**: 3573–3584. doi:10.1016/S0016-7037(02)00968-7

Li, M., Y. J. Lee, J. M. Testa, Y. Li, W. Ni, W. M. Kemp, and D. M. Di Toro. 2016. What drives interannual variability of hypoxia in Chesapeake Bay: Climate forcing versus nutrient loading? Geophys. Res. Lett. **43**: 2127–2134. doi:10.1002/2015GL067334

Linker, L. C., R. A. Batiuk, C. F. Cerco, G. W. Shenk, R. Tian, P. Wang, and G. Yactayo. 2016. Influence of reservoir infill on coastal deep water hypoxia. J. Environ. Qual. **45**: 887–893. doi:10.2134/jeq2014.11.0461

Loh, A. N., J. E. Bauer, and E. A. Canuel. 2006. Dissolved and particulate organic matter source-age characterization in the upper and lower Chesapeake Bay: A combined isotope and biochemical approach. Limnol. Oceanogr. **51**: 1421–1431. doi:10.4319/lo.2006.51.3.1421

Lustwerk, R. L., and D. J. Burdige. 1993. Iron and manganese reduction in Chesapeake Bay sediments. Trans. Am. Geophys. Union (EOS) **74**: 326.

Meade, R. H. 1969. Landward transport of bottom sediments in estuaries of the Atlantic coastal plain. J. Sediment. Res. **39**: 222–234. doi:10.1306/74d71c1c-2b21-11d7-8648000102c1865d

Millero, F. J. 1991*a*. The oxidation of H_2S in Black Sea waters. Deep-Sea Res. Part A Oceanogr. Res. Pap. **38**: S1139–S1150. doi:10.1016/S0198-0149(10)80028-7

Millero, F. J. 1991*b*. The oxidation of H_2S in the Chesapeake Bay. Estuar. Coast. Shelf Sci. **33**: 521–527. doi:10.1016/0272-7714(91)90088-S

Mucci, A. 1983. The solubility of calcite and aragonite in seawater at various salinities, temperatures, and one atmosphere total pressure. Am. J. Sci. **283**: 780–799. doi:10.2475/ajs.283.7.780

Murphy, R. R., W. M. Kemp, and W. P. Ball. 2011. Long-term trends in Chesapeake Bay seasonal hypoxia, stratification, and nutrient loading. Estuaries Coast. **34**: 1293–1309. doi:10.1007/s12237-011-9413-7

Najjar, R. G., and others. 2010. Potential climate-change impacts on the Chesapeake Bay. Estuar. Coast. Shelf Sci. **86**: 1–20. doi:10.1016/j.ecss.2009.09.026

Officer, C. B. 1979. Discussion of the behaviour of nonconservative dissolved constituents in estuaries. Estuar. Coast. Mar. Sci. **9**: 91–94. doi:10.1016/0302-3524(79)90009-4

Officer, C. B., R. B. Biggs, J. L. Taft, L. E. Cronin, M. A. Tyler, and W. R. Boynton. 1984. Chesapeake Bay anoxia: Origin, development, and significance. Science **223**: 22–27. doi:10.1126/science.223.4631.22

Orr, J. C., and others. 2005. Anthropogenic Ocean acidification over the twenty-first century and its impact on calcifying organisms. Nature **437**: 681. doi:10.1038/nature04095

Orth, R. J., and others. 2017. Submersed aquatic vegetation in Chesapeake Bay: Sentinel species in a changing world. Bioscience **67**: 698–712. doi:10.1093/biosci/bix058

Paerl, H. W. 2006. Assessing and managing nutrient-enhanced eutrophication in estuarine and coastal waters: Interactive effects of human and climatic perturbations. Ecol. Eng. **26**: 40–54. doi:10.1016/j.ecoleng.2005.09.006

Pai, S. C., G. C. Gong, and K. K. Liu. 1993. Determination of dissolved oxygen in seawater by direct spectrophotometry of total iodine. Mar. Chem. **41**: 343–351. doi:10.1016/0304-4203(93)90266

Pilson, M. E. 2012. An introduction to the chemistry of the sea. Cambridge Univ. Press.

Presley, B. J., and I. R. Kaplan. 1968. Changes in dissolved sulfate, calcium and carbonate from interstitial water of nearshore sediments. Geochim. Cosmochim. Acta **32**: 1037–1048. doi:10.1016/0016-7037(68)90106-3

Qian, W., and others. 2018. Current status of emerging hypoxia in a eutrophic estuary: The lower reach of the Pearl River Estuary, China. Estuar. Coast. Shelf Sci. **205**: 58–67. doi:10.1016/j.ecss.2018.03.004

Quay, P., R. Sonnerup, J. Stutsman, J. Maurer, A. Körtzinger, X. A. Padin, and C. Robinson. 2007. Anthropogenic CO_2 accumulation rates in the North Atlantic Ocean from changes in the $^{13}C/^{12}C$ of dissolved inorganic carbon. Global Biogeochem. Cycles **21**: GB1009. doi:10.1029/2006GB002761

Rabalais, N. N., R. J. Díaz, L. A. Levin, R. E. Turner, D. Gilbert, and J. Zhang. 2010. Dynamics and distribution of natural and human-caused hypoxia. Biogeosciences **7**: 585–619. doi:10.5194/bg-7-585-2010

Rabalais, N. N., and others. 2014. Eutrophication-driven deoxygenation in the coastal ocean. Oceanography **27**: 172–183. doi:10.5670/oceanog.2014.21

Rabouille, C., and others. 2008. Comparison of hypoxia among four river-dominated ocean margins: The Changjiang (Yangtze), Mississippi, Pearl, and Rhône rivers. Cont. Shelf Res. **28**: 1527–1537. doi:10.1016/j.csr.2008.01.020

Rassmann, J., E. M. Eitel, C. Cathalot, C. Brandily, B. Lansard, M. Taillefert, and C. Rabouille. 2019. Benthic alkalinity and DIC fluxes in the Rhône River prodelta generated by decoupled aerobic and anaerobic processes. Biogeosci. Discuss. **2019**: 1–50. doi:10.5194/bg-2019-32

Redfield, A. C. 1934. On the proportions of organic derivatives in sea water and their relation to the composition of plankton, p. 176–192. *In* R. J. Daniel [ed.], James Johnstone memorial volume. Liverpool Univ. Press.

Roden, E. E., and J. H. Tuttle. 1992. Sulfide release from estuarine sediments underlying anoxic bottom water. Limnol. Oceanogr. **37**: 725–738. doi:10.4319/lo.1992.37.4.0725

Roden, E. E., and J. H. Tuttle. 1993. Inorganic sulfur cycling in mid and lower Chesapeake Bay sediments. Mar. Ecol. Prog. Ser. **93**: 101–118. doi:10.3354/meps093101

Roden, E. E., J. H. Tuttle, W. R. Boynton, and W. M. Kemp. 1995. Carbon cycling in mesohaline Chesapeake Bay sediments 1: POC deposition rates and mineralization pathways. J. Mar. Res. **53**: 779–819. doi:10.1357/0022240953213025

Samanta, S., T. K. Dalai, J. K. Pattanaik, S. K. Rai, and A. Mazumdar. 2015. Dissolved inorganic carbon (DIC) and its $\delta^{13}C$ in the Ganga (Hooghly) River Estuary, India: Evidence of DIC generation via organic carbon degradation and carbonate dissolution. Geochim. Cosmochim. Acta **165**: 226–248. doi:10.1016/j.gca.2015.05.040

Sampou, P., and C. A. Oviatt. 1991. Seasonal patterns of sedimentary carbon and anaerobic respiration along a simulated eutrophication gradient. Mar. Ecol. Prog. Ser. **72**: 271–282. doi:10.3354/meps072271

Sanford, L. P., S. E. Suttles, and J. P. Halka. 2001. Reconsidering the physics of the Chesapeake Bay estuarine turbidity maximum. Estuaries **24**: 655–669. doi:10.2307/1352874

Schubel, J., and D. Pritchard. 1986. Responses of upper Chesapeake Bay to variations in discharge of the Susquehanna River. Estuaries **9**: 236–249. doi:10.2307/1352096

Shen, C., J. M. Testa, W. Ni, W.-J. Cai, M. Li, and W. M. Kemp. 2019*a*. Ecosystem metabolism and carbon balance in Chesapeake Bay: A 30-year analysis using a coupled hydrodynamic-biogeochemical model. J. Geophys. Res. Oceans **124**: 6141–6153. doi:10.1029/2019jc015296

Shen, C., and others. 2019*b*. Controls on carbonate system dynamics in a coastal plain estuary: A modeling study. J. Geophys. Res. Biogeosci. **124**: 61–78. doi:10.1029/2018jg004802

Shultz, D. J., and J. A. Calder. 1976. Organic carbon $^{13}C/^{12}C$ variations in estuarine sediments. Geochim. Cosmochim. Acta **40**: 381–385. doi:10.1016/0016-7037(76)90002-8

Sigleo, A. C., and S. A. Macko. 2002. Carbon and nitrogen isotopes in suspended particles and colloids, Chesapeake and San Francisco Estuaries, U.S.A. Estuar. Coast. Shelf Sci. **54**: 701–711. doi:10.1006/ecss.2001.0853

Smith, E. M., and W. M. Kemp. 1995. Seasonal and regional variations in plankton community production and respiration for Chesapeake Bay. Mar. Ecol. Prog. Ser. **116**: 217–231. doi:10.3354/meps116217

Stevenson, J. C., M. S. Kearney, and E. C. Pendleton. 1985. Sedimentation and erosion in a Chesapeake Bay brackish marsh system. Mar. Geol. **67**: 213–235. doi:10.1016/0025-3227(85)90093-3

Stevenson, J. C., L. G. Ward, and M. S. Kearney. 1988. Sediment transport and trapping in marsh systems: Implications of tidal flux studies. Mar. Geol. **80**: 37–59. doi:10.1016/0025-3227(88)90071-0

Stribling, J. M., and J. C. Cornwell. 1997. Identification of important primary producers in a Chesapeake Bay tidal creek system using stable isotopes of carbon and sulfur. Estuaries **20**: 77–85. doi:10.2307/1352721

Strong, D. J., and others. 2012. Organic matter distribution in the modern sediments of the Pearl River Estuary. Org. Geochem. **49**: 68–82. doi:10.1016/j.orggeochem.2012.04.011

Su, J., M. Dai, B. He, L. Wang, J. Gan, X. Guo, H. Zhao, and F. Yu. 2017. Tracing the origin of the oxygen-consuming organic matter in the hypoxic zone in a large eutrophic estuary: The lower reach of the Pearl River Estuary, China. Biogeosciences **14**: 4085–4099. doi:10.5194/bg-14-4085-2017

Su, J., W.-J. Cai, N. Hussain, J. Brodeur, B. Chen, and K. Huang. 2019. Simultaneous determination of dissolved inorganic carbon (DIC) concentration and stable isotope ($\delta^{13}C$-DIC) by Cavity Ring-Down Spectroscopy: Application to study carbonate dynamics in the Chesapeake Bay. Mar. Chem. **215**: 103689. doi:10.1016/j.marchem.2019.103689

Swarzenski, P., P. Campbell, L. Osterman, and R. Poore. 2008. A 1000-year sediment record of recurring hypoxia off the Mississippi River: The potential role of terrestrially-derived organic matter inputs. Mar. Chem. **109**: 130–142. doi:10.1016/j.marchem.2008.01.003

Testa, J. M., D. C. Brady, D. M. Di Toro, W. R. Boynton, J. C. Cornwell, and W. M. Kemp. 2013. Sediment flux modeling: Simulating nitrogen, phosphorus, and silica cycles. Estuar. Coast. Shelf Sci. **131**: 245–263. doi:10.1016/j.ecss.2013.06.014

Testa, J. M., and W. M. Kemp. 2014. Spatial and temporal patterns of winter–spring oxygen depletion in Chesapeake Bay bottom water. Estuaries Coast. **37**: 1432–1448. doi:10.1007/s12237-014-9775-8

Testa, J. M., W. M. Kemp, and W. R. Boynton. 2018*a*. Season-specific trends and linkages of nitrogen and oxygen cycles in Chesapeake Bay. Limnol. Oceanogr. **63**: 2045–2064. doi:10.1002/lno.10823

Testa, J. M., R. R. Murphy, D. C. Brady, and W. M. Kemp. 2018*b*. Nutrient- and climate-induced shifts in the phenology of linked biogeochemical cycles in a temperate estuary. Front. Mar. Sci. **5**: 114. doi:10.3389/fmars.2018.00114

Thornton, S. F., and J. McManus. 1994. Application of organic carbon and nitrogen stable isotope and C/N ratios as source indicators of organic matter provenance in estuarine systems: Evidence from the Tay Estuary, Scotland. Estuar. Coast. Shelf Sci. **38**: 219–233. doi:10.1006/ecss.1994.1015

Turner, R. E., and N. N. Rabalais. 1994. Coastal eutrophication near the Mississippi river delta. Nature **368**: 619–621. doi:10.1038/368619a0

Wang, H., X. Hu, N. N. Rabalais, and J. Brandes. 2018. Drivers of oxygen consumption in the northern Gulf of Mexico hypoxic waters—a stable carbon isotope perspective. Geophys. Res. Lett. **45**: 10528–10538. doi:10.1029/2018GL078571

Wolf-Gladrow, D. A., R. E. Zeebe, C. Klaas, A. Körtzinger, and A. G. Dickson. 2007. Total alkalinity: The explicit conservative expression and its application to biogeochemical processes. Mar. Chem. **106**: 287–300. doi:10.1016/j.marchem.2007.01.006

Wu, R. S. 2002. Hypoxia: From molecular responses to ecosystem responses. Mar. Pollut. Bull. **45**: 35–45. doi:10.1016/S0025-326X(02)00061-9

Xu, Y.-Y., D. Pierrot, and W.-J. Cai. 2017*a*. Ocean carbonate system computation for anoxic waters using an updated CO2SYS program. Mar. Chem. **195**: 90–93. doi:10.1016/j.marchem.2017.07.002

Xu, Y.-Y., and others. 2017*b*. Short-term variability of aragonite saturation state in the central Mid-Atlantic Bight. J. Geophys. Res. Oceans **122**: 4274–4290. doi:10.1002/2017JC012901

Yu, F., Y. Zong, J. M. Lloyd, G. Huang, M. J. Leng, C. Kendrick, A. L. Lamb, and W. W.-S. Yim. 2010. Bulk organic $\delta^{13}C$ and C/N as indicators for sediment sources in the Pearl River delta and estuary, southern China. Estuar. Coast. Shelf Sci. **87**: 618–630. doi:10.1016/j.ecss.2010.02.018

Zhang, J., Z. G. Yu, J. T. Wang, J. L. Ren, H. T. Chen, H. Xiong, L. X. Dong, and W. Y. Xu. 1999. The Subtropical Zhujiang (Pearl River) Estuary: Nutrient, trace species and their relationship to photosynthesis. Estuar. Coast. Shelf Sci. **49**: 385–400. doi:10.1006/ecss.1999.0500

Zhao, H.-D., S.-J. Kao, W.-D. Zhai, K.-P. Zang, N. Zheng, X.-M. Xu, C. Huo, and J.-Y. Wang. 2017. Effects of stratification, organic matter remineralization and bathymetry on summertime oxygen distribution in the Bohai Sea, China. Cont. Shelf Res. **134**: 15–25. doi:10.1016/j.csr.2016.12.004

Acknowledgments

This work was supported by NOAA grant. We thank the captain and the crew of R/V *Rachel Carson* for their cooperation during the cruise. We thank Casey Hodgkins for assistance on the field work, and Yafeng Zhang for TA sample measurements. This is UMCES publication number 5735.

Conflict of Interest

None declared.

Submitted 29 May 2019
Revised 19 November 2019
Accepted 09 January 2020

Associate editor: Bo Thamdrup